ORIGINAL ARTICLE

A collinearity diagnosis of the GNSS geocenter determination

Paul Rebischung · Zuheir Altamimi · Tim Springer

Abstract The problem of observing geocenter motion from global navigation satellite system (GNSS) solutions through the network shift approach is addressed from the perspective of collinearity (or multicollinearity) among the parameters of a least-squares regression. A collinearity diagnosis, based on the notion of variance inflation factor, is therefore developed and allows handling several peculiarities of the GNSS geocenter determination problem. Its application reveals that the determination of all three components of geocenter motion with GNSS suffers from serious collinearity issues, with a comparable level as in the problem of determining the terrestrial scale simultaneously with the GNSS satellite phase center offsets. The inability of current GNSS, as opposed to satellite laser ranging, to properly sense geocenter motion is mostly explained by the estimation, in the GNSS case, of epoch-wise station and satellite clock offsets simultaneously with tropospheric parameters. The empirical satellite accelerations, as estimated by most Analysis Centers of the International GNSS Service, slightly amplify the collinearity of the Z geocenter coordinate, but their role remains secondary.

Keywords GNSS · SLR · Geocenter · Collinearity · Multicollinearity · Variance inflation factor · Correlation

P. Rebischung (✉) · Z. Altamimi
IGN LAREG, Univ Paris Diderot, Sorbonne Paris Cité,
5 rue Thomas Mann, 75205 Paris Cedex 13, France
e-mail: paul.rebischung@ign.fr

T. Springer
European Space Operations Centre (ESOC), Robert-Bosch-Strasse 5,
64293 Darmstadt, Germany

1 Introduction

Geocenter motion is usually defined, with varying sign conventions, as the relative motion between the center of mass of the total Earth system (CM) and the center of figure of the solid Earth surface (CF). Its geophysical cause is the redistribution of masses within the Earth system, from daily and sub-daily periods (e.g. ocean tides) to secular time scales (e.g. post-glacial rebound, present-day ice melting) via seasonal and inter-annual periods (e.g. water mass exchanges). As Earth satellites orbit around CM, geocenter motion affects the measurements of surface processes made by geodetic satellites. An accurate determination of geocenter motion is therefore required for the most demanding geodetic applications. While the tidal part of geocenter motion is part of the IERS Conventions (Petit and Luzum 2010), the accurate determination of its non-tidal part remains challenging. We refer the reader to Wu et al. (2012) for a detailed description of geocenter motion and of its implications.

There currently exists two conceptual approaches for monitoring geocenter motion. The first one, often called network shift approach, or translational approach, relies on satellite tracking data. Since Earth satellites orbit CM, global sets of station-satellite range measurements for given periods (e.g. days, weeks or months) can be used to infer the tracking station coordinates in theoretically CM-centered frames. The origin of the International Terrestrial Reference Frame (ITRF) is obtained through a long-term stacking of such CM-centered frames derived from Satellite Laser Ranging (SLR) measurements and therefore theoretically follows CM on the long term. On the other hand, the translations between quasi-instantaneous CM-centered frames and the ITRF should reflect the non-secular part of geocenter motion (Dong et al. 2003; Collilieux et al. 2009).

The second approach, often called deformation approach, or degree-1 approach, was first proposed by Blewitt et al. (2001). It is based on the fact that geocenter motions due to surface mass redistributions are accompanied by deformations of the Earth's crust. Such deformations can be accurately monitored using global networks of GNSS stations, which allows an indirect observation of geocenter motion. The deformation approach can however only sense non-secular geocenter motions induced by surface load variations and can therefore not help in defining the ITRF origin.

This article entirely focuses on the network shift approach. As it is the only approach capable of sensing secular geocenter motion, its performance is critical for the observation of long-term geophysical processes like global sea level rise, post-glacial rebound or present-day ice melting. Any inaccuracy in the long-term following of CM by the ITRF origin does in particular directly translate into errors in the estimation of global sea-level rise by satellite altimetry (Morel and Willis 2005; Beckley et al. 2007) or by global tide-gauge records and GPS (Collilieux and Wöppelmann 2011). While a stability of 0.1 mm/year is aimed for the ITRF origin, external evaluations of the origin of ITRF2008 (Altamimi et al. 2011) assessed its stability to a level of 0.5 mm/year (Wu et al. 2011; Collilieux 2013), or even 0.9 mm/year along the Z axis (Argus 2012). The performance of the network shift approach therefore still needs to be improved.

There currently exists three satellite tracking techniques theoretically capable of sensing geocenter motion through the network shift approach: SLR, DORIS and GNSS. However, only one of them, SLR, gives relatively satisfying results and contributes to the definition of the ITRF origin. DORIS-derived geocenter time series recently benefited from tremendous improvements, but remain much noisier than SLR-derived series, especially in the Z component (Gobinddass et al. 2009a,b). Finally, the GNSS technique, although benefits from the largest satellite constellation and tracking network, has so far not proven able to reliably observe geocenter motion through the network shift approach.

Collilieux et al. (2011), indeed, analyzed the translation time series between reprocessed weekly solutions provided by four Analysis Centers (ACs) of the International GNSS Service (IGS; Dow et al. 2009) and a preliminary version of ITRF2008. Significant long-term biases were noted with respect to the SLR translations, as well as AC-dependent trends in the Z component. Moreover, the annual signals present in the X and Z components of the IGS AC translation time series were in poor agreement with SLR. A frequency analysis of the IGS AC translation time series finally revealed that all were contaminated by spurious periodic signals at harmonics of the GPS draconitic year (351.5 days; Ray et al. 2008) with amplitudes reaching several millimetres. The question underlying this article is therefore: Why are current GNSS, despite their numerous satellites and dense track-ing networks, unable to reliably observe geocenter motion through the network shift approach?

This question was recently addressed through orbital perturbation considerations by Meindl et al. (2013). The same question is addressed in this article from the perspective of *collinearity* (also known as *multicollinearity*). Collinearity in a least-squares regression can be defined as the existence of quasi-linear dependencies among the parameters. Its consequence is that some linear combinations of parameters are extremely sensitive to observation and model errors and may therefore not be reliably inferred from the observations. This article demonstrates that the inability of GNSS to reliably observe geocenter motion is precisely due to such a collinearity problem.

Section 2 gives a brief introduction to the least-squares regression method, to the issue of collinearity among least-squares parameters and to the notion of variance inflation factor. The collinearity diagnosis at the basis of the article is then presented in its simplest form. In Sect. 3, this collinearity diagnosis is generalized so as to handle several peculiarities of the GNSS geocenter determination problem. A practical method for performing collinearity diagnoses in global GNSS analyses is then given. Section 4 gives a concrete example of our generalized collinearity diagnosis, with its application to the well-known quasi-singular problem of determining the terrestrial scale simultaneously with the GNSS satellite phase center offsets. Section 5 describes in detail the *signatures* of the geocenter coordinates on satellite tracking observations. Finally, our collinearity diagnosis is respectively applied in Sects. 6 and 7 to the geocenter determination with SLR and GNSS.

2 Mathematical background

This section introduces the basic mathematical notions used throughout the article. After a brief introduction to least-squares regression and to the issue of collinearity in least-squares regression, the collinearity diagnosis at the basis of the article is then presented in its simplest form.

2.1 Least-squares regression

Consider the linear regression model $l = Ax + v$, where:

- l is a vector of n observations with given covariance matrix $Q_l = P_l^{-1}$;
- x a vector of p unknown parameters;
- $A = \partial l / \partial x$ is the so-called design matrix (the ith column of A will be denoted A_i in the following);
- Ax is the vector of observations predicted by the parameters x (model prediction);
- v is a vector of unknown observational and model errors (residuals).

Specifying a weight matrix P_l for the observations corresponds to the choice of a particular metric in the observation space $\mathbb{R}^n$, i.e. of an inner product $\langle l, l' \rangle = l^T P_l l'$ and of the associated norm $\|l\| = \sqrt{l^T P_l l}$. Let E denote the Hilbert observation space $\mathbb{R}^n$ equipped with this metric. The column space of the design matrix, $\text{Im}(A) = \{Ax, x \in \mathbb{R}^p\}$, is a subspace of E which spans all possible model predictions. It will therefore be called the model space.

The objective of a least-squares regression is to minimize the norm $\|v\| = \|l - Ax\|$ of the residual vector. It is achieved when the vector of predicted observations Ax is the orthogonal projection of the observation vector l onto the model space $\text{Im}(A)$. This condition leads to the well-known normal equation:

$$Nx = b \tag{1}$$

where $N = A^T P_l A$ is called the normal matrix and $b = A^T P_l l$. When A is of full rank, N is invertible and the normal equation has a unique solution:

$$\hat{x} = N^{-1} b = (A^T P_l A)^{-1} A^T P_l l \tag{2}$$

The covariance matrix of the estimated parameters is in this case the inverse of the normal matrix: $Q = N^{-1}$. The goodness of fit can be measured by the coefficient of determination:

$$R^2 = \frac{\|A\hat{x}\|^2}{\|l\|^2} = \cos^2 \theta \tag{3}$$

where θ is the angle between the observation vector l and the model space $\text{Im}(A)$.

2.2 Conditioning and parameter scaling

When A is of full rank but N is however close to singularity, small perturbations in the observations may cause relatively large variations in the estimated parameters: the least-squares regression is ill conditioned. The closeness of N to singularity can be measured by its condition number $\kappa(N)$, i.e. the ratio of its largest to its smallest singular value.

Because N is symmetric, the ideal case $\kappa(N) = 1$ is achieved only when:

$$N = kI \iff \begin{cases} \forall i, & N_{i,i} = \|A_i\|^2 = k \\ \forall i \neq j, N_{i,j} = \langle A_i, A_j \rangle = 0 \end{cases} \tag{4}$$

i.e. when the columns of A form an orthogonal basis of the model space $\text{Im}(A)$ and all have the same norm. N can thus be ill conditioned for two non-exclusive reasons: either because the columns of A have disparate norms (scaling problem), or because they are far from being orthogonal to each other (collinearity problem).

The first possible reason for ill conditioning can be circumvented by solving for an auxiliary set of scaled parameters $\tilde{x}$ such that $\tilde{x}_i = \|A_i\| x_i = \sqrt{N_{i,i}} x_i$. In matrix notations, $\tilde{x} = \tilde{D}^{-1} x$ where $\tilde{D}$ denotes the diagonal matrix with elements $\tilde{D}_{i,i} = 1/\sqrt{N_{i,i}}$. This leads to the design matrix $\tilde{A} = A\tilde{D}$ whose columns all have unit norms, and to the scaled normal equation $\tilde{N}\tilde{x} = \tilde{b}$, where $\tilde{N} = \tilde{D} N \tilde{D}$ has the form of a correlation matrix and $\tilde{b} = \tilde{D}b$.

In terms of condition number, this particular scaling of the parameters may not be optimal: there may exist other matrices D in the set $\mathcal{D}_p$ of all non-singular $p \times p$ diagonal matrices such that $\kappa(DND) < \kappa(\tilde{N})$. Nevertheless, a theorem by van der Sluis (1969) states that:

$$\kappa(\tilde{N}) \leq p \min_{D \in \mathcal{D}_p} \kappa(DND) \tag{5}$$

i.e. even if the scaling by $\tilde{D}$ is not optimal, it is not far from being optimal. But the main justification for this particular scaling is that it isolates the second possible source for ill conditioning: collinearity.

2.3 Collinearity

When the design matrix A is rank deficient, there exists one or more linear dependencies among its columns. One or more linear combinations of the parameters are not observable, i.e. cannot be inferred from the observations. The normal matrix N is consequently singular. We will refer to this situation, well known in geodetic problems, as perfect collinearity.

More subtly, the columns of A may be, not exactly, but nearly linearly dependent, meaning that some linear combinations of the parameters are only hardly observable. This situation, namely collinearity, or multicollinearity, translates into a large condition number for the scaled normal matrix $\tilde{N}$. Geometrically, collinearity can be defined as a severe departure of the basis formed by the columns of $\tilde{A}$ from orthogonality (Farrar and Glauber 1967), or as the closeness of this basis to singularity (Haitovsky 1969).

The harm caused by collinearity to the estimability of specific linear combinations of parameters is described as follows by Belsley et al. (1980): "The essential harm due to collinearity arises from the fact that a collinear relation can readily result in a situation in which some of the observed systematic influence of the explanatory variables on the response variable is swamped by the models random error term—or in the familiar terminology of electrical engineering, the signal is swamped by the noise. It is intuitively clear that, under these circumstances, estimation can be hindered."

Belsley et al. (1980) (see also Belsley (1991)) also suggest a procedure, based on the singular value decomposition of $\tilde{N}$, to identify near dependencies among the columns of $\tilde{A}$ and the parameters involved in them. The application of Belsley's procedure to global GNSS solutions would certainly be rich of lessons. However, because a parameter is

generally involved, at different levels, in all eigenvectors of $\tilde{N}$, Belsley's procedure does not appear to us as the most appropriate tool to understand *why* a specific parameter is affected by collinearity, i.e. the mechanism that makes this parameter hardly observable. As the questions underlying this article are whether and, if so, *why* the GNSS geocenter determination is harmed by collinearity, we will thus prefer another diagnosis involving the notion of variance inflation factor (VIF).

2.4 Diagnosing the collinearity of a specific parameter

It will be assumed throughout this section that A is of full rank, so that its columns form a basis of the model space $\text{Im}(A)$.

Signature of a parameter Each column $A_i = \partial l / \partial x_i$ of A is a vector of the model space, which represents the effect on the observations predicted by the model of a unit variation of the ith parameter x_i. In the following, A_i will be called the *signature* of x_i on the observations.

Decomposition of A_i Each parameter x_i can also be associated with a particular hyperplane of the model space. Let $e_i = [\delta_{i,1}, \delta_{i,2}, \ldots, \delta_{i,p}]^{\text{T}}$ (vector with all zero elements, except a unit ith element) be the coordinates of x_i in the canonical basis of the parameter space $\mathbb{R}^p$. Let K_i be any $p \times p - 1$ matrix whose columns form a basis of $\text{Ker}(e_i^{\text{T}}) = \{x \in \mathbb{R}^p / e_i^{\text{T}} x = 0\}$. One could choose for instance:

$$K_i = [e_1, \ldots, e_{i-1}, e_{i+1}, \ldots, e_p] \tag{6}$$

$\text{Im}(AK_i)$ is the $p - 1$ dimensional subspace (hyperplane) of the model space, which contains the signatures of all parameters except x_i.

Let us now decompose the signature A_i of x_i into the sum of its orthogonal projection A_i^u onto $\text{Im}(AK_i)$ and of

Fig. 1 Decomposition of the signature of x_3 in a three-parameter problem. $\text{Im}(AK_3)$ is the plane containing A_1 and A_2. A_3^u is the orthogonal projection of A_3 onto this plane. A_3^p is the orthogonal projection of A_3 onto the line orthogonal to this plane. θ_3 is the angle between A_3 and this plane

its orthogonal projection A_i^p onto $\text{Im}(AK_i)^{\perp}$ (Fig. 1). A_i^u, as it lies in $\text{Im}(AK_i)$, is strictly collinear with the signatures of $x_1, \ldots, x_{i-1}, x_{i+1}, \ldots x_p$. This part of the signature of x_i is consequently indistinguishable from the signatures of the other parameters. The estimation of x_i can therefore only rely on A_i^p (part of A_i which is orthogonal to each of the signatures of $x_1, \ldots, x_{i-1}, x_{i+1}, \ldots x_p$). In the following, A_i^p will be called the *proper signature* of x_i. It can be expressed as:

$$A_i^p = \frac{A Q e_i}{Q_{i,i}} \tag{7}$$

Equation (7) is a particular case of Eq. (19) introduced in Sect. 3.1 and proven in Appendix B (Online Resource).

Variance inflation factor Let us associate to each parameter x_i the angle θ_i between its signature A_i and the hyperplane $\text{Im}(AK_i)$ (Fig. 1). $R_i^2 = \cos^2 \theta_i$ is the coefficient of determination obtained from the regression of A_i on the other columns of A. The variance inflation factor (VIF) of x_i is defined from the angle θ_i, or from R_i^2, by:

$$V_i = \frac{1}{\sin^2 \theta_i} = \frac{1}{1 - R_i^2} \tag{8}$$

$V_i = 1$ ($\theta_i = \pi/2$; $R_i^2 = 0$) means that A_i is orthogonal to all other columns of A, i.e. x_i is uncorrelated with any other parameter. On the other hand, V_i tends to infinity ($\theta_i \to 0$; $R_i^2 \to 1$) when A_i tends to lie in $\text{Im}(AK_i)$ and x_i tends to be unobservable. V_i thus measures the degree of collinearity of x_i with all other parameters.

VIFs are a well-established tool for diagnosing whether the estimation of specific parameters may be harmed by collinearity (see, e.g., Farrar and Glauber 1967; Belsley et al. 1980; Draper and Smith 1998; Montgomery et al. 2012). The term "variance inflation factor", introduced by Marquardt (1970), derives from the fact that the variance of a parameter x_i obeys the relation:

$$\text{var}(\hat{x}_i) = Q_{i,i} = \frac{1}{N_{i,i}} . V_i \tag{9}$$

The first factor, $1/N_{i,i}$, would be the variance of x_i if all other parameters were held fixed. V_i is thus the factor by which the presence of the other parameters inflates the variance of x_i. Equation (9) can be demonstrated by noting that:

$$\cos \theta_i = \frac{\langle A_i, A_i^u \rangle}{\|A_i\| \|A_i^u\|} = \frac{\langle A_i, A_i - A_i^p \rangle}{\|A_i\| \|A_i - A_i^p\|} \tag{10}$$

Replacing A_i^p by its expression in Eq. (7) leads to:

$$\cos \theta_i = \sqrt{1 - \frac{1}{N_{i,i} Q_{i,i}}} \tag{11}$$
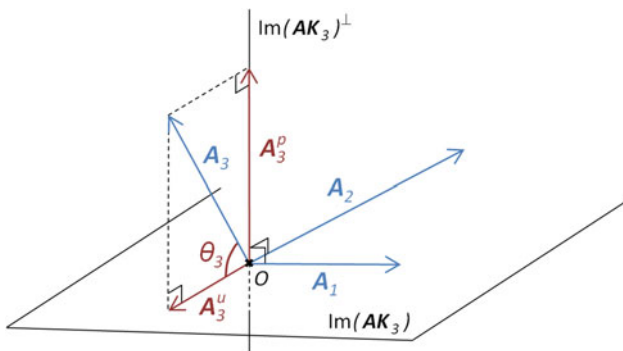
which is equivalent to Eq. (9).

Let us mention another interpretation of VIFs. Using Eq. (7), it can be shown that:

$$V_i = \frac{\|A_i\|^2}{\|A_i^p\|^2} \quad (12)$$

The numerator in Eq. (12) is the squared norm of the signature of x_i on the observations, i.e. of the signal on which the estimation of x_i would rely if all other parameters were held fixed. On the other hand, the denominator in Eq. (12) is the squared norm of the *proper* signature of x_i, i.e. of the signal on which the estimation of x_i actually relies. V_i thus measures how the magnitude of the signal on which the estimation of x_i relies is reduced because of the estimation of other parameters.

When analysing VIFs, one inevitably runs into the questions of what are large and what are small VIFs. Numerical thresholds are given in the literature, commonly seen values being 5 and 10 (see, e.g., Montgomery et al. 2012). But they are essentially arbitrary and probably not suited to problems with thousands of parameters, like global GNSS analyses. Note, finally, that because of their quotient nature, VIFs should be considered as varying on a logarithmic scale rather than on a linear scale.

For the ease of interpretation, numerical VIF values will always be accompanied, in the rest of the article, by bracketed percentage values corresponding to:

$$\cos \theta_i = R_i = \sqrt{1 - \frac{1}{V_i}} \quad (13)$$

By its nature, this quantity is indeed interpretable in the same way as a correlation coefficient.

Coordinates of A_i^u. When analysing the collinearity of x_i with the other parameters, not only the values of θ_i, R_i^2 and V_i are of interest, but also the coordinates of A_i^u in the basis formed by the columns of A. If x_i has a large VIF (small θ_i), A_i^u is indeed a linear combination of $A_1, \ldots, A_{i-1}, A_{i+1}, \ldots A_p$ which closely matches A_i. In other words, the coordinates of A_i^u in the basis formed by the columns of A are the coefficients of a linear combination of $x_1, \ldots, x_{i-1}, x_{i+1}, \ldots x_p$ which is almost indistinguishable from x_i. The coordinates of A_i^u are thus the answer to the question of why x_i may be hardly observable.

According to Eq. (8),

$$A_i^u = A_i - A_i^p = A \left(e_i - \frac{Q e_i}{Q_{i,i}} \right) \quad (14)$$

so that the coordinates γ_i of A_i^u in the basis formed by the columns of A are:

$$\begin{aligned}\gamma_i &= e_i - \frac{Q e_i}{Q_{i,i}} \\ &= -\left[\frac{Q_{1,i}}{Q_{i,i}}, \ldots, \frac{Q_{i-1,i}}{Q_{i,i}}, 0, \frac{Q_{i+1,i}}{Q_{i,i}}, \ldots, \frac{Q_{p,i}}{Q_{i,i}} \right]^{\mathrm{T}}\end{aligned} \quad (15)$$

3 Adaptations to the GNSS geocenter determination problem

Before the collinearity diagnosis exposed in Sect. 2.4 can be applied to the GNSS geocenter determination problem, some adaptations and further developments are first needed due to several peculiarities of global GNSS analyses.

The first difficulty comes from the fact that geocenter coordinates are usually not estimated as explicit parameters in GNSS solutions, for they would be fully redundant with station coordinates. Geocenter coordinates are rather implicitly realized through station coordinates. Section 3.1 will therefore propose a generalization of the notions introduced in Sect. 2.4 to such "implicit parameters".

Secondly, unlike that assumed in the end of Sect. 2, it is well-known that the design matrix of a global GNSS problem is not of full rank (perfect collinearity). Rotations of the terrestrial frame can indeed be compensated by variations of the Earth orientation parameters (EOPs), so that A has three orientation singularities. A fourth singularity stems from the correlation of the UT1-UTC offset with the longitudes of the orbit ascending nodes. In the presence of such singularities, straightforwardly computed VIFs would be infinite and useless for many parameters (including geocenter coordinates). Section 3.2 will therefore propose a way of performing meaningful collinearity diagnoses when A is not of full rank.

Lastly, a practical difficulty arises from the large number of parameters in global GNSS problems. A typical daily GPS solution with 100 stations, 30 satellites, 5-min sampled undifferenced observations and all phase cycle ambiguities fixed indeed includes nearly 41,000 parameters, 92 % of which are epoch-wise estimated satellite and station clock offsets. These clock parameters are usually either reduced from the normal equation, or annihilated by the use of double-differenced observations, both methods being equivalent under certain conditions (Appendix F, Online Resource). The practical question answered in Sect. 3.3 is then: How can collinearity diagnoses be made without disposing of the whole normal matrix?

Another question one could legitimately ask is whether the geocenter determination and the potentially related collinearity issues are equivalent in the undifferenced and double-differenced processing methods. The answer follows of course immediately from the equivalence of both methods themselves. But we will make this equivalence even clearer with a relationship between "undifferenced VIFs" and "double-differenced VIFs" (Sect. 3.4).

3.1 Collinearity diagnosis for implicit parameters

The purpose of this section is to generalize the collinearity diagnosis exposed in Sect. 2.4 to quantities which are, like geocenter coordinates, not estimated as explicit model para-

meters, but implicitly realized through the model parameters. It is again assumed in this section that A and N are of full rank.

Implicit parameters Let us define an implicit parameter as a quantity y whose impact of a unit variation on the observations predicted by the model (signature) is a known vector of the model space:

$$S_y = \frac{\partial l}{\partial y} = A\lambda \tag{16}$$

For instance, in a global GNSS problem, the signature of the implicit parameter corresponding to the X coordinate of the geocenter is:

$$A \underbrace{[1, 0, 0, 1, 0, 0, \dots, 1, 0, 0,}_{\text{station coordinates}} \underbrace{0, 0, 0, 0, \dots, 0]^{\mathrm{T}}}_{\text{other parameters}} \tag{17}$$

i.e. the impact on the observations predicted by the model of a unit X translation of the station network. Explicit model parameters are encompassed by the notion of implicit parameter. The signature of x_i on the observations predicted by the model is indeed a known vector of the model space: $\partial l / \partial x_i = A_i = A e_i$.

When A is of full rank, a unit variation of an implicit parameter y, i.e. a variation $\delta l = S_y = A\lambda$ of the observations, can be univocally associated with a variation:

$$\delta x = N^{-1} A^{\mathrm{T}} P_l \delta l = \lambda \tag{18}$$

of the estimated model parameters. λ can thus be interpreted as the vector of partial derivatives of the explicit model parameters with respect to y: $\lambda = \partial x / \partial y$.

Independence of two implicit parameters Two implicit parameters y and z, characterized, respectively by $\partial x / \partial y = \lambda$ and $\partial x / \partial z = \mu$ will be said to be independent if $\lambda^{\mathrm{T}} \mu = 0$, i.e. if λ and μ are orthogonal in the parameter space $\mathbb{R}^p$. Orthogonality in the parameter space may be thought in terms of degrees of freedom allowed within the model. For example, two explicit parameters x_i and x_j are clearly allowed to vary independently from each other within the model: $e_i^{\mathrm{T}} e_j = 0$. On the other hand, a quantity like $x_i + x_j$ cannot vary independently from x_i: $e_i^{\mathrm{T}}(e_i + e_j) \neq 0$. More generally, $\lambda^{\mathrm{T}} \mu = 0$ means that the implicit parameters y and z can vary independently from each other within the model.

Decomposition of S_y Let K_y denote any $p \times p - 1$ matrix whose columns form a basis of $\mathrm{Ker}(\lambda^{\mathrm{T}})$. Provided that A is of full rank, $\mathrm{Im}(A K_y)$ is a $p - 1$ dimensional subspace (hyperplane) of the model space $\mathrm{Im}(A)$ which spans the signatures of all implicit parameters independent of y. The signature S_y of y can be decomposed into the sum of its orthogonal projection S_y^u onto $\mathrm{Im}(A K_y)$ and of its orthogonal projection S_y^p onto $\mathrm{Im}(A K_y)^\perp$. S_y^u, as it lies in $\mathrm{Im}(A K_y)$, can be exactly reproduced by the signatures of implicit parameters

independent of y, i.e. that are allowed to vary independently of y within the model. The estimation of y can therefore only rely on S_y^p, which will be called the *proper signature* of y. Appendix B (Online Resource) proves that S_y^p can be expressed as:

$$S_y^p = \frac{\lambda^{\mathrm{T}} \lambda}{\lambda^{\mathrm{T}} Q \lambda} A Q \lambda \tag{19}$$

VIF of an implicit parameter Let θ_y denote the angle between the signature S_y of y and the hyperplane $\mathrm{Im}(A K_y)$. Using Eq. (19), it can be shown that:

$$\cos \theta_y = \frac{\langle S_y, S_y^u \rangle}{\|S_y\| \|S_y^u\|} = \frac{\langle S_y, S_y - S_y^p \rangle}{\|S_y\| \|S_y - S_y^p\|}$$
$$= \sqrt{1 - \frac{(\lambda^{\mathrm{T}} \lambda)^2}{(\lambda^{\mathrm{T}} N \lambda)(\lambda^{\mathrm{T}} Q \lambda)}} \tag{20}$$

One can also show that, if a regression of S_y on the columns of $A K_y$ was made, the obtained coefficient of determination would be $R_y^2 = \cos^2 \theta_y$.

The variance inflation factor V_y of an implicit parameter y can be defined from θ_y or R_y^2 by:

$$V_y = \frac{1}{\sin^2 \theta_y} = \frac{1}{1 - R_y^2} \tag{21}$$

Inserting Eq. (20) into Eq. (21) leads to a formula from which V_y can be practically computed when disposing of the normal matrix N and of its inverse Q:

$$V_y = \frac{(\lambda^{\mathrm{T}} N \lambda)(\lambda^{\mathrm{T}} Q \lambda)}{(\lambda^{\mathrm{T}} \lambda)^2} \tag{22}$$

Replacing λ by e_i in the preceding developments leads back to the equations of Sect. 2.4, which proves that this extension of VIFs to implicit parameters encompasses usual VIFs.

The interpretation of such generalized VIFs remains the same. $V_y = 1$ when S_y is orthogonal to $\mathrm{Im}(A K_y)$, i.e. when y is uncorrelated with any other independent implicit parameter. On the other hand, V_y tends to infinity when S_y tends to lie in $\mathrm{Im}(A K_y)$ and y tends to be unobservable. Note that V_y is still interpretable as a "variance inflation factor". No proof is however given here; further developments would be needed to properly define the variance of an implicit parameter. Let us finally mention that V_y can still be interpreted as the ratio of the squared norm of the signature of y on the observations to the squared norm of its proper signature. Using Eqs. (16) and (19), one can in fact show that:

$$V_y = \frac{\|S_y\|^2}{\|S_y^p\|^2} \tag{23}$$

Coordinates of S_y^u Like the coordinates of A_i^u in the basis formed by the columns of A can enlighten why a parameter x_i may be hardly observable, the coordinates of S_y^u in this

basis can similarly explain why an implicit parameter y is hardly observable. These coordinates can now be interpreted as $\boldsymbol{\mu} = \partial \boldsymbol{x} / \partial z$ where z is the implicit parameter independent of y whose signature $\boldsymbol{S}_z = \boldsymbol{S}_y^u$ most closely matches $\boldsymbol{S}_y$.

According to Eqs. (16) and (19),

$$S_y^u = S_y - S_y^p = A \left(\boldsymbol{\lambda} - \frac{\boldsymbol{\lambda}^{\mathrm{T}} \boldsymbol{\lambda}}{\boldsymbol{\lambda}^{\mathrm{T}} \boldsymbol{Q} \boldsymbol{\lambda}} \boldsymbol{Q} \boldsymbol{\lambda} \right) \quad (24)$$

so that the coordinates $\boldsymbol{\gamma}_y$ of $\boldsymbol{S}_y^u$ in the basis formed by the columns of $\boldsymbol{A}$ are:

$$\boldsymbol{\gamma}_y = \boldsymbol{\lambda} - \frac{\boldsymbol{\lambda}^{\mathrm{T}} \boldsymbol{\lambda}}{\boldsymbol{\lambda}^{\mathrm{T}} \boldsymbol{Q} \boldsymbol{\lambda}} \boldsymbol{Q} \boldsymbol{\lambda} \quad (25)$$

3.2 Collinearity diagnosis in the presence of singularities and minimal constraints

In many geodetic problems, the design matrix $\boldsymbol{A}$ is not of full rank, so that the normal matrix $\boldsymbol{N}$ is not invertible. The formulas derived in Sect. 3.1, as they involve the inverse $\boldsymbol{Q}$ of the normal matrix, are therefore clearly not usable. Another view of the problem is that, when $\boldsymbol{A}$ is not of full rank, an implicit parameter y can generally not be univocally associated with a specific variation of the model parameters. A third view of the problem is that, because of the singularities of $\boldsymbol{A}$, the subspace $\mathrm{Im}(\boldsymbol{A}\boldsymbol{K}_y)$ defined in Sect. 3.1 is not necessarily a hyperplane of the model space, but can be the model space $\mathrm{Im}(\boldsymbol{A})$ itself. This section therefore proposes a way of performing meaningful collinearity diagnoses when $\boldsymbol{A}$ is not of full rank, and more precisely in the case where minimal constraints are used to supplement the rank deficiencies of $\boldsymbol{A}$.

Minimal constraints When $\boldsymbol{A}$ and $\boldsymbol{N}$ have $c > 0$ singularities, a well-established practice in geodesy consists in augmenting the normal equation with minimal constraints. This leads to a system of the form:

$$\begin{bmatrix} \boldsymbol{N} & \boldsymbol{C} \\ \boldsymbol{C}^{\mathrm{T}} & \boldsymbol{0} \end{bmatrix} \begin{bmatrix} \boldsymbol{x}_c \\ \boldsymbol{k} \end{bmatrix} = \begin{bmatrix} \boldsymbol{b} \\ \boldsymbol{0} \end{bmatrix} \quad (26)$$

where

- $\boldsymbol{C}^{\mathrm{T}}$ is a $c \times p$ full-rank constraint matrix such that rank$[\boldsymbol{N}\ \boldsymbol{C}] = p$;
- $\boldsymbol{k}$ is a vector of c Lagrange multipliers.

In global GNSS problems, the constraint matrix classically has the form:

$$\boldsymbol{C}^{\mathrm{T}} = \begin{vmatrix} \ldots & 0 & -Z_i & Y_i & \ldots & 0 & 0 & \ldots & 0 \\ \ldots & Z_i & 0 & -X_i & \ldots & 0 & 0 & \ldots & 0 \\ \ldots & -Y_i & X_i & 0 & \ldots & 0 & 0 & \ldots & 0 \\ \ldots & 0 & 0 & 0 & \ldots & 1 & 0 & \ldots & 0 \end{vmatrix}$$

$$\underbrace{}_{\text{station coordinates}} \underbrace{}_{\text{UT1-UTC}} \text{other parameters}$$

$$(27)$$

The first three lines impose that the orientation of the estimated terrestrial frame be the same as that of the a priori frame (no-net-rotation constraint). The fourth line directly fixes the UT1-UTC offset to its a priori value.

Blaha (1971) shows that the augmented normal equation (26) has a unique solution $\hat{\boldsymbol{x}}_c$ which minimizes $\|\boldsymbol{v}\| = \|\boldsymbol{l} - \boldsymbol{A}\boldsymbol{x}_c\|$ under the condition (constraint) that $\boldsymbol{C}^{\mathrm{T}} \boldsymbol{x}_c = \boldsymbol{0}$. He also proves that the covariance matrix $\boldsymbol{Q}_c$ of $\hat{\boldsymbol{x}}_c$ is the upper-left block of the inverse of the augmented normal matrix. Appendix C (Online Resource) shows that $\hat{\boldsymbol{x}}_c$ and $\boldsymbol{Q}_c$ can be expressed as:

$$\hat{\boldsymbol{x}}_c = \boldsymbol{B}(\boldsymbol{B}^{\mathrm{T}} \boldsymbol{N} \boldsymbol{B})^{-1} \boldsymbol{B}^{\mathrm{T}} \boldsymbol{b} \quad (28)$$

$$\boldsymbol{Q}_c = \boldsymbol{B}(\boldsymbol{B}^{\mathrm{T}} \boldsymbol{N} \boldsymbol{B})^{-1} \boldsymbol{B}^{\mathrm{T}} \quad (29)$$

where $\boldsymbol{B}$ denotes any $p \times p - c$ matrix whose columns form a basis of $\mathrm{Ker}(\boldsymbol{C}^{\mathrm{T}})$.

Note that we use the term "constraints" in the same sense as Blaha (1971), i.e. as a synonym for "condition equations". Another common acceptance of this term refers to the introduction of weighted pseudo-observations, which would lead to a normal equation of type $(\boldsymbol{N} + \boldsymbol{C}\boldsymbol{P}_c\boldsymbol{C}^{\mathrm{T}})\boldsymbol{x} = \boldsymbol{b}$. Although this latter method is generally preferred in practice, we adopt here the condition equation approach for its mathematical appeal. Condition equations are in fact equivalent to pseudo-observations with infinite weights.

Implicit parameters Let y be an implicit parameter defined by its signature $\boldsymbol{S}_y = \boldsymbol{A}\boldsymbol{\lambda}$ on the observations. When $\boldsymbol{A}$ is not of full rank, but minimal constraints are used, y can again be univocally associated with a specific variation of the model parameters. According to Eq. (28), a unit variation of y, i.e. a variation $\boldsymbol{\delta l} = \boldsymbol{S}_y = \boldsymbol{A}\boldsymbol{\lambda}$ of the observations, indeed leads to a variation:

$$\boldsymbol{\delta x}_c = \boldsymbol{B}(\boldsymbol{B}^{\mathrm{T}} \boldsymbol{N} \boldsymbol{B})^{-1} \boldsymbol{B}^{\mathrm{T}} \boldsymbol{A}^{\mathrm{T}} \boldsymbol{P}_l \boldsymbol{\delta l}$$
$$= \boldsymbol{B}(\boldsymbol{B}^{\mathrm{T}} \boldsymbol{N} \boldsymbol{B})^{-1} \boldsymbol{B}^{\mathrm{T}} \boldsymbol{N} \boldsymbol{\lambda} \quad (30)$$

of the estimated parameters. In other words, the partial derivatives $\boldsymbol{\lambda}_c$ of the model parameters with respect to y are:

$$\boldsymbol{\lambda}_c = \frac{\partial \boldsymbol{x}_c}{\partial y} = \boldsymbol{B}(\boldsymbol{B}^{\mathrm{T}} \boldsymbol{N} \boldsymbol{B})^{-1} \boldsymbol{B}^{\mathrm{T}} \boldsymbol{N} \boldsymbol{\lambda} = \boldsymbol{Q}_c \boldsymbol{N} \boldsymbol{\lambda} \quad (31)$$

$\boldsymbol{\lambda}_c$ is in fact the unique solution of the system:

$$\begin{cases} \boldsymbol{A}\boldsymbol{\lambda}_c = \boldsymbol{A}\boldsymbol{\lambda} \\ \boldsymbol{C}^{\mathrm{T}}\boldsymbol{\lambda}_c = \boldsymbol{0} \end{cases} \quad (32)$$

It can therefore be interpreted as the unique variation of the model parameters which is allowed by the constraints and has the same signature on the observations as y.

The notion of independence between implicit parameters remains unchanged: y and z are independent if the corresponding parameter variations $\lambda_c = \partial x_c / \partial y$ and $\mu_c = \partial x_c / \partial z$ are orthogonal in the parameter space. For a given y and λ_c, the set of such μ_cs is Ker$([\lambda_c \ C]^T)$.

Decomposition of S_y Let $K_{y,c}$ denote any matrix whose columns form a basis of Ker$([\lambda_c \ C]^T)$. It is proven in Appendix D (Online Resource) that as long as $\lambda \notin$ Ker(A), Im$(A K_{y,c})$ is a $p - c - 1$ dimensional subspace (hyperplane) of the model space. As previously, the signature S_y of y can then be decomposed into the sum of its orthogonal projection $S_{y,c}^u$ onto Im$(A K_{y,c})$ and of its orthogonal projection $S_{y,c}^p$ onto Im$(A K_{y,c})^\perp$. $S_{y,c}^u$ is indistinguishable from the signatures of implicit parameters independent of y. The estimation of y can therefore only rely on its proper signature $S_{y,c}^p$. Appendix D (Online Resource) proves that it can be expressed as:

$$S_{y,c}^p = \frac{\lambda_c^T \lambda_c}{\lambda_c^T Q_c \lambda_c} A Q_c \lambda_c \tag{33}$$

Variance inflation factors When A is not of full rank and minimal constraints are used, the variance inflation factor of an implicit parameter y can be defined from the angle $\theta_{y,c}$ between its signature and the hyperplane Im$(A K_{y,c})$ by:

$$V_{y,c} = \frac{1}{\sin^2 \theta_{y,c}} \tag{34}$$

Using Eq. (33), it can be shown that:

$$\cos \theta_{y,c} = \frac{\langle S_y, S_{y,c}^u \rangle}{\|S_y\| \|S_{y,c}^u\|} = \frac{\langle S_y, S_y - S_{y,c}^p \rangle}{\|S_y\| \|S_y - S_{y,c}^p\|}$$
$$= \sqrt{1 - \frac{(\lambda_c^T \lambda_c)^2}{(\lambda_c^T N \lambda_c)(\lambda_c^T Q_c \lambda_c)}} \tag{35}$$

This leads to a formula from which $V_{y,c}$ can be practically computed when disposing of N and Q_c:

$$V_{y,c} = \frac{(\lambda_c^T N \lambda_c)(\lambda_c^T Q_c \lambda_c)}{(\lambda_c^T \lambda_c)^2} \tag{36}$$

As previously, $V_{y,c}$ can be interpreted as the ratio of the squared norm of the signature of y on the observations to the squared norm of its proper signature. Using Eq. (33) and the fact that $A\lambda = A\lambda_c$, one can in fact show that:

$$V_y = \frac{\|S_y\|^2}{\|S_{y,c}^p\|^2} \tag{37}$$

Coordinates of $S_{y,c}^u$ According to Eq. (33), $S_{y,c}^u$ can be expressed as:

$$S_{y,c}^u = S_y - S_{y,c}^p = A \left(\lambda_c - \frac{\lambda_c^T \lambda_c}{\lambda_c^T Q_c \lambda_c} Q_c \lambda_c \right) \tag{38}$$

The vector

$$\gamma_{y,c} = \lambda_c - \frac{\lambda_c^T \lambda_c}{\lambda_c^T Q_c \lambda_c} Q_c \lambda_c \tag{39}$$

can be interpreted as $\partial x_c / \partial z$ where z is the implicit parameter independent of y whose signature most closely matches S_y. It can therefore explain why an implicit parameter y may be hardly observable.

3.3 Practical method for collinearity diagnoses

The expressions of $V_{y,c}$ and $\gamma_{y,c}$ given in Sect. 3.2 involve the full normal matrix N and the full covariance matrix of the parameters Q_c. However, in a standard global undifferenced GNSS analysis, station and satellite clock parameters are generally reduced, so that neither N nor Q_c are fully computed. A practical way for obtaining $V_{y,c}$ and $\gamma_{y,c}$ is therefore exposed in this section.

Parameter reduction Assume that the vector of parameters can be split into $x = [x_1^T \ x_2^T]^T$ where x_1 contains parameters of interest, while x_2 contains "nuisance parameters" (e.g. clock offsets). A constrained normal equation like Eq. (26) can be block-decomposed into:

$$\begin{bmatrix} N_{11} & N_{12} & C_1 \\ N_{21} & N_{22} & C_2 \\ C_1^T & C_2^T & 0 \end{bmatrix} \begin{bmatrix} x_1 \\ x_2 \\ k \end{bmatrix} = \begin{bmatrix} b_1 \\ b_2 \\ 0 \end{bmatrix} \tag{40}$$

If N_{22} is invertible, solving Eq. (40) is equivalent to solving the reduced normal equation:

$$\begin{bmatrix} N_{11} - N_{12} N_{22}^{-1} N_{21} & C_1 - N_{12} N_{22}^{-1} C_2 \\ C_1^T - C_2^T N_{22}^{-1} N_{21} & -C_2^T N_{22}^{-1} C_2 \end{bmatrix} \begin{bmatrix} x_1 \\ k \end{bmatrix}$$
$$= \begin{bmatrix} b_1 - N_{12} N_{22}^{-1} b_2 \\ -C_2^T N_{22}^{-1} b_2 \end{bmatrix} \tag{41}$$

and "back-solving" x_2 by:

$$x_2 = N_{22}^{-1}(b_2 - N_{21} x_1 - C_2 k) \tag{42}$$

This reduction method is widely employed in undifferenced GNSS analyses. It avoids the storage and inversion of the full normal matrix N. Moreover, since x_2 consists of epoch clock parameters, N_{22} has a block-diagonal structure which makes it efficiently invertible.

Computing λ_c Consider an implicit parameter y defined by its signature $S_y = A\lambda$ on the observations. The first step in our practical method for diagnosing the collinearity of y consists in computing the partial derivatives $\lambda_c = \partial x_c / \partial y$ of the model parameters with respect to y. From Eqs. (28) and

(31), it is easily seen that $\boldsymbol{\lambda}_c$ is the solution of the following normal equation:

$$\begin{bmatrix} N & C \\ C^{\mathrm{T}} & 0 \end{bmatrix} \begin{bmatrix} x_c \\ k \end{bmatrix} = \begin{bmatrix} N\lambda \\ 0 \end{bmatrix} = \begin{bmatrix} A^{\mathrm{T}} P_l S_y \\ 0 \end{bmatrix} \tag{43}$$

which can be reduced and efficiently solved.

Computing $\boldsymbol{\gamma}_{y,c}$ Consider the following system:

$$\begin{bmatrix} N & C & \lambda_c \\ C^{\mathrm{T}} & 0 & 0 \\ \lambda_c^{\mathrm{T}} & 0 & 0 \end{bmatrix} \begin{bmatrix} x_c \\ k \\ k' \end{bmatrix} = \begin{bmatrix} 0 \\ 0 \\ \lambda_c^{\mathrm{T}} \lambda_c \end{bmatrix} \tag{44}$$

Its solution minimizes $\|Ax_c\|$ under the constraint that $C^{\mathrm{T}} x_c = 0$ and the additional condition that $\lambda_c^{\mathrm{T}} x_c = \lambda_c^{\mathrm{T}} \lambda_c$. This latter condition is equivalent to imposing a unit change of y with respect to the a priori parameters. On the other hand, the minimization of $\|Ax_c\|$ means that the observations predicted by the estimated parameters should stay as close as possible to the observations predicted by the a priori parameters. In other words, an artificial unit error in y is introduced, but the system tries to compensate its impact on the observations as much as possible.

Appendix E (Online Resource) proves that the solution of Eq. (44) is $\boldsymbol{\lambda}_c - \boldsymbol{\gamma}_{y,c}$. The first term, $\boldsymbol{\lambda}_c$ represents the artificially introduced error, while the second term, $-\boldsymbol{\gamma}_{y,c}$, is the best solution found by the system to compensate the impact of this error on the observations. Equation (44) can also be reduced and efficiently solved. $\boldsymbol{\gamma}_{y,c}$ can then be obtained from its solution.

Computing $V_{y,c}$ The last remaining step is a practical method for computing the VIF $V_{y,c}$ of y. For that purpose, let us rearrange Eq. (37) into:

$$V_{y,c} = \frac{\|S_y\|^2}{\|S_{y,c}^p\|^2} = \frac{\|A\lambda_c\|^2}{\|A(\lambda_c - \gamma_{y,c})\|^2} \tag{45}$$

This last expression shows how to obtain $V_{y,c}$ from $A\boldsymbol{\lambda}_c$ and $A(\boldsymbol{\lambda}_c - \boldsymbol{\gamma}_{y,c})$. In practice, the full design matrix A may not be available, but $A\boldsymbol{\lambda}_c$ and $A(\boldsymbol{\lambda}_c - \boldsymbol{\gamma}_{y,c})$ can nevertheless be computed by evaluating the model function at the set of a priori parameters x_0, at $x_0 + \boldsymbol{\lambda}_c$ and at $x_0 + \boldsymbol{\lambda}_c - \boldsymbol{\gamma}_{y,c}$.

3.4 Impact of double-differencing on VIFs

It is shown in Appendix F (Online Resource) that, as long as a maximal set of independent double-differenced observations is used, the double differencing approach leads to an identical normal equation as the reduction of clock parameters. The use of double-differenced observations rather than undifferenced observations has therefore no theoretical impact on the GNSS geocenter determination problem. One could nevertheless compute VIFs directly from a double-differenced system and would obtain different values as with the full undifferenced system. We therefore deem it important to explain the relationship between such double-differenced and undifferenced VIFs.

Suppose that a maximal set of independent double-differenced observations $\boldsymbol{l}_d$ is obtained from the undifferenced observations $\boldsymbol{l}$ through the application of an $n_d \times n$ differencing operator $\boldsymbol{D}$: $\boldsymbol{l}_d = \boldsymbol{D}\boldsymbol{l}$. The weight matrix of the double-differenced observations:

$$\boldsymbol{P}_{l_d} = \boldsymbol{Q}_{l_d}^{-1} = (\boldsymbol{D} \boldsymbol{Q}_l \boldsymbol{D}^{\mathrm{T}})^{-1} \tag{46}$$

induces the norm $\|\boldsymbol{l}_d\|_d = \sqrt{\boldsymbol{l}_d^{\mathrm{T}} \boldsymbol{P}_{l_d} \boldsymbol{l}_d}$ in the space of double-differenced observations $\mathbb{R}^{n_d}$. Consider an implicit parameter y defined by its signature $\boldsymbol{S}_y$ on the undifferenced observations. The signature of y on the double-differenced observations is $\boldsymbol{S}_{y,d} = \boldsymbol{D}\boldsymbol{S}_y$. Appendix G (Online Resource) proves that the VIFs V_y and $V_{y,d}$, obtained, respectively in the undifferenced and in the double-differenced cases are related by:

$$\frac{V_{y,d}}{V_y} = \frac{\|S_{y,d}\|_d^2}{\|S_y\|^2} \tag{47}$$

This fraction is also proven to be always smaller than 1.

The left term in Eq. (47) represents a reduction of the collinearity of y with the other parameters in the double-differenced case. This reduction naturally stems from the fact that a double-differenced system has less parameters than an undifferenced system. On the other hand, the right term in Eq. (47) represents a loss of sensitivity to y due to double-differencing the observations. In summary, the formation of double differences has the apparent advantage of reducing collinearity among parameters, but this advantage is in fact totally offset by a reduction of the sensitivity of the observations.

Equation (47) can in particular be used to quantify the sensitivity reduction to geocenter coordinates qualitatively observed by Meindl et al. (2013) when forming double differences. This sensitivity reduction can equivalently be thought in terms of collinearity of the geocenter coordinates with satellite and station clock offsets. In the following, we will prefer undifferenced observations for their simpler geometric interpretation and adopt the latter point of view.

4 Application to the GNSS terrestrial scale determination problem

Because of:

– a high correlation between the terrestrial scale and the satellite radial phase center offsets (z-PCOs) (Zhu et al. 2003; Cardellach et al. 2007),

Table 1 Simulation options

Aspect	Option
Station network	Fictive network of 100 well-distributed stations
Constellation	24 satellites on 6 orbital planes $a = 26{,}560$ km, $e = 0$, $i = 55°$
Data span	24 h
Observation sampling	5 min
Cutoff angle	10°
Observation weighting	All observations equally weighted

Table 2 List of simulated parameters

Type	Number
Station coordinates	3 per station
Zenithal wet delays (ZWDs)	1 per station and hour
Tropospheric gradients	2 per station
Station clock offsets	1 per station and epoch
Satellite initial state vectors	6 per satellite
Satellite empirical accelerations	5 per satellite
Satellite clock offsets	1 per satellite and epoch
Satellite z-PCOs	1 per satellite
EOPs	6

– the fact that pre-launch phase center offset calibrations are not available for any of the GPS and GLONASS satellites launched so far,

current GNSS are considered unable to provide terrestrial scale information and do not contribute to the definition of the ITRF scale (Altamimi et al. 2011). On the contrary, the IGS currently relies on the ITRF scale to determine conventional GPS and GLONASS z-PCOs (Ray et al. 2013; Rebischung et al. 2012).

The collinearity diagnosis developed in Sect. 3 is applied in this section to this well-known problem, mainly with an illustrative purpose. The VIFs obtained for the terrestrial scale will also serve as references for interpreting the VIFs obtained in Sect. 7 for the geocenter coordinates.

4.1 Signature of a terrestrial scale change

Let us consider the implicit parameter y corresponding to a terrestrial scale change of $\delta s = 1$ ppb. The signature of y on a set of GNSS observations is $\boldsymbol{S}_y = \boldsymbol{A}\boldsymbol{\lambda}$ with:

$$\boldsymbol{\lambda} = \delta s \,[\underbrace{\ldots, X_i, Y_i, Z_i, \ldots,}_{\text{station coordinates}} \underbrace{0, 0, 0, 0, \ldots, 0}_{\text{other parameters}}]^{\mathrm{T}} \qquad (48)$$

$\boldsymbol{\lambda}$ corresponds to a change of the geocentric radius (height) of any station by $\delta r \simeq a_{\mathrm{E}} \delta s \simeq 6.4$ mm, where a_{E} denotes

the mean Earth radius. The impact of such a height change on an observation l made at an elevation angle e is $\delta l = -\delta r \sin(e) \simeq -a_{\mathrm{E}} \delta s \sin(e)$. The elements of $\boldsymbol{S}_y$ are nothing but such δls.

4.2 Simulation

Using the options listed in Table 1, a series of observations (station-satellite ranges) was simulated and a design matrix including the parameters listed in Table 2 was set up. The considered satellite empirical accelerations are the five terms of the Extended CODE Orbit Model (ECOM) (Beutler et al. 1994; Springer 1999) estimated by most of the IGS Analysis Centers (ACs): D_0, Y_0, B_0, B_c and B_s using the notations of Rodriguez-Solano et al. (2012). The considered EOPs are the pole coordinates x_p and y_p at noon, their rates $\dot{x}_p$ and $\dot{y}_p$, the UT1-UTC offset at noon and the length-of-day (LOD). Note that simple mapping functions have been used for ZWDs $(1/\sin(e))$ and tropospheric gradients (from Chen and Herring 1997). Also note that a zero-mean condition has been applied at each epoch to all satellite and station clock offsets.

Except satellite z-PCOs, the list of parameters in Table 2 is the minimal common set of parameters freely estimated by a majority of IGS ACs. It could in fact be the list of parameters set up by a slightly sub-standard AC. The collinearity diagnoses exposed in the following will be based on this particular sub-standard list of parameters. But note that the estimation of additional parameters (e.g. satellite velocity pulses, additional empirical accelerations, but also unfixed phase cycle ambiguities) by the real ACs can only increase collinearity issues.

The satellite z-PCOs are usually set up, but tightly constrained by the IGS ACs. In the simulations of this section, they are however freely estimated for the particular purpose of studying their collinearity with the terrestrial scale.

Except the fictive station network and constellation, the options listed in Table 1 could also be those used by an IGS AC. The choice of a perfectly distributed network and constellation was made to avoid perturbing the obtained results by some "network effect". But additional simulations with real network and constellation will also be performed for comparison in Sect. 4.4. The influence of the cutoff angle and of the observation weighting will similarly be investigated through additional simulations in Sect. 4.4.

4.3 Collinearity diagnosis

Equation (43) was then solved, leading to $\boldsymbol{\lambda}_c = \partial \boldsymbol{x}_c / \partial y$, i.e. the impact of a 1 ppb scale change on the estimated parameters under no-net-rotation constraints. Because a perfectly distributed station network was used, $\boldsymbol{\lambda}_c$ was in fact equal to $\boldsymbol{\lambda}$.
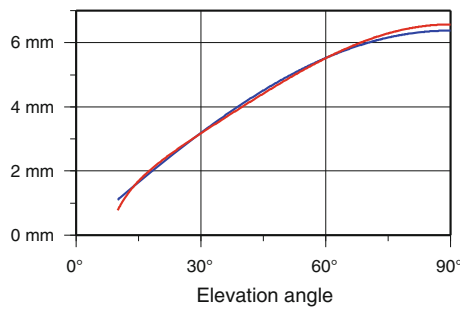
Fig. 2 *Blue* opposite of the impact on the observations of a 1 ppb scale change, plotted as a function of the elevation angle ($a_E \delta s \sin(e)$). *Red* sum of the impacts on the observations of the obtained clock, ZWD and z-PCO mean variations, plotted as a function of the elevation angle $\left(130.09 + 0.40/\sin e - 137.06\sqrt{1 - a_E^2 \cos^2 e / a^2}\right)$

Fig. 3 *Left* signature of a 1 ppb scale change on the observations made by a particular station, represented as a skyplot. Each *dot* represents an element of $S_y = A\lambda_c$. *Right* corresponding proper signature. Each *dot* represents an element of $S_{y,c}^p = A(\lambda_c - \gamma_{y,c})$. Note the different color scales

Equation (44) was finally solved. A 1 ppb scale change with respect to the a priori terrestrial frame was imposed through the additional constraint $\lambda_c^T x_c = \lambda_c^T \lambda_c$. But the system compensated it as much as possible through an independent variation $-\gamma_{y,c}$ of the parameters. The obtained parameter variation $-\gamma_{y,c}$ was composed of:

– a mean variation of the satellite z-PCOs by -137.06 mm, plus small satellite-specific z-PCO variations below 0.23 mm,
– a mean variation of the satellite clock offsets by -25.18 mm (-83.99 ps), plus small satellite- and epoch-specific variations below 0.43 mm (1.43 ps),
– a mean variation of the station clock offsets by 104.91 mm, plus small station- and epoch-specific variations below 0.29 mm,
– a mean variation of the ZWDs by -0.40 mm, plus small station- and hour-specific variations below 0.11 mm.

The other parameters (station coordinates, tropospheric gradients and satellite orbit parameters) were not significantly affected.

The obtained mean variation of the satellite and station clock offsets has the effect of shortening the predicted observations by $-25.18 - 104.91 = -130.09$ mm. The impact of the obtained mean ZWD variation is to shorten any observation made at an elevation e by $-0.40/\sin e$ mm. Finally, according to Cardellach et al. (2007), the impact of the obtained mean z-PCO variation is to lengthen any observation made at an elevation e by $137.06\sqrt{1 - a_E^2 \cos^2 e / a^2}$ mm. The sum of these three effects is compared in Fig. 2 with the impact on the observations of the introduced terrestrial scale change.

Figure 2 shows that the impact of the introduced terrestrial scale change could be almost perfectly compensated by variations of independent parameters (clock offsets, ZWDs and z-PCO), which indicates a severe collinearity of the terres-
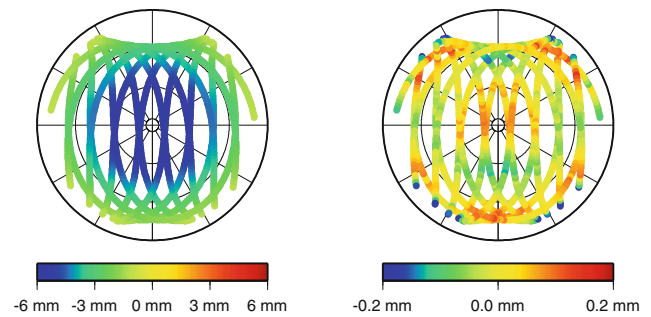
trial scale with those parameters. Another view of the same result is given in Fig. 3, where the signature of a 1 ppb terrestrial scale change on the observations made by a particular station is compared to the corresponding proper signature. There is a reduction by almost two orders of magnitude from the signature to the proper signature of the terrestrial scale change, which also points to a severe collinearity issue.

The VIF obtained for the terrestrial scale in this simulation was in fact 3,076.9 ($\sqrt{1 - 1/\text{VIF}} = 99.984$ %), far beyond the commonly seen thresholds of 5 (89.443 %) and 10 (94.868 %).

4.4 Complementary simulations

A second simulation was run with the same options as previously, except that the satellite z-PCOs were held fixed. The obtained VIF was 47.2 (98.935 %). When the satellite z-PCOs are not estimated, clock offsets and ZWDs are much less able to compensate the introduced terrestrial scale change. The collinearity of the terrestrial scale with the other parameters is thus greatly reduced.
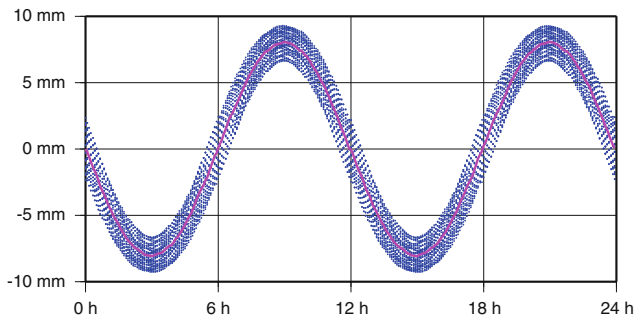
Another simulation based on a real network of 150 stations and a real constellation of 30 GPS satellites (both extracted from a solution provided by ESA for July 11, 2008) was run, with all other options as described in Sect. 4.2. The obtained VIF was 3,123.9 (99.984 %), just slightly above the VIF obtained with a perfectly distributed station network and constellation. The mechanism described in Sect. 4.3 holds in fact for any network and constellation. The distribution of the station network and of the constellation does not seem to have a significant impact on the collinearity of the terrestrial scale with the other parameters, as long as satellite z-PCOs are estimated.

The impacts of the cutoff angle and of the observation weighting were finally investigated through different simulations. The obtained VIFs are given in Table 3. The collinearity of the terrestrial scale with the other parameters clearly

Table 3 VIFs obtained for the terrestrial scale with different cutoff angles and observation weighting functions

Weighting function	Cutoff angle			
	0°	5°	10°	20°
1	86.0 (99.417 %)	706.2 (99.929 %)	3,076.9 (99.984 %)	46,439.2 (99.999 %)
$\sin e$	316.3 (99.842 %)	1,520.8 (99.967 %)	5,214.1 (99.990 %)	58,784.4 (99.999 %)
$\sin^2 e$	1,462.5 (99.966 %)	3,652.0 (99.986 %)	9,622.2 (99.995 %)	79,083.3 (99.999 %)

The other simulation options were as described in Sect. 4.2

Fig. 4 Signature of a 1 cm Z geocenter shift on simulated observations made on a GPS-like satellite by the whole station network. Each *blue dot* represents an element of S_y. The *magenta line* is an epoch mean

Fig. 5 Signature of a 1 cm Z geocenter shift on simulated observations made by five particular stations. An epoch mean signature was first removed for each satellite

increases when higher cutoff angles are used. This translates the fact that the more the signature of the terrestrial scale change ($-a_E \delta s \sin(e)$; blue curve in Fig. 2) is truncated, the more accurately it can be matched by linear combinations of the partial derivatives of clock offsets, z-PCOs and ZWDs. Downweighting low elevation observations similarly increases the collinearity of the terrestrial scale with the other parameters.
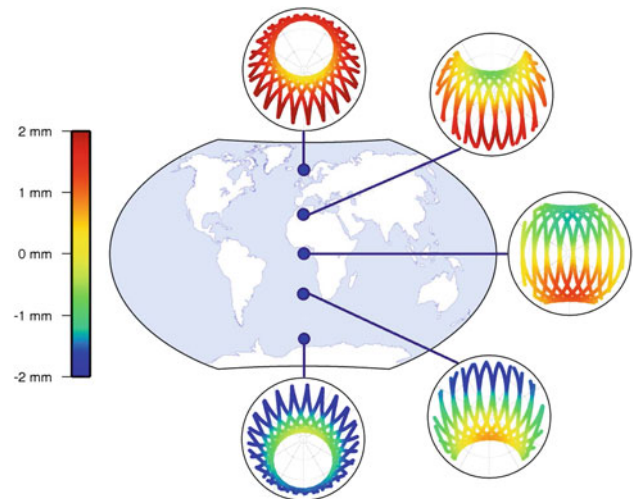
5 Signature of geocenter shifts on station-satellite ranges

As a last preliminary step before investigating the collinearity of the geocenter coordinates with other GNSS parameters, this section describes the signature of geocenter shifts on station-satellite range observations. The impact of a geocenter shift along the Z axis is first studied, followed by the impacts of geocenter shifts along the X and Y axes of the terrestrial frame.

5.1 Signature of a Z geocenter shift

Consider the implicit parameter y corresponding to a geocenter shift of $\delta t = 1$ cm along the Z axis. The signature of y on a set of observations is $S_y = A\lambda$ with:

$$\lambda = [\underbrace{0, 0, \delta t, \dots, 0, 0, \delta t}_{\text{station coordinates}}, \underbrace{0, 0, 0, 0, \dots, 0}_{\text{other parameters}}]^T \qquad (49)$$

This signature was computed for the particular set of observations described in Sect. 4.2. It is represented in Fig. 4 from the point of view of a particular satellite.

The impact of a positive Z geocenter shift is basically to shorten the observations made when the satellite is in the Northern hemisphere and to lengthen the observations made when the satellite is in the Southern hemisphere. That is why, at first order, the signature of a positive Z geocenter shift follows the opposite of the satellite Z coordinate. For a circular orbit, this results in a sinusoid with an amplitude $\delta t \sin i$, where i denotes the inclination of the satellite orbit.

The "width" of the blue sinusoid in Fig. 4 stems from the fact that, at a given epoch, observations are made on the same satellite by several stations under different angles, and are thus differently affected by the geocenter shift. This width mainly depends on the radius of the satellite orbit, but also of the employed cutoff angle.

With slight anticipation over Sect. 7, let us mention that the epoch mean signature shown in magenta in Fig. 4 can be strictly compensated by variations of the satellite clock offsets and is therefore unobservable in a standard GNSS analysis. The determination of the Z geocenter coordinate with GNSS can consequently only rely on the difference between its signature and this epoch mean signature (i.e. on the signal
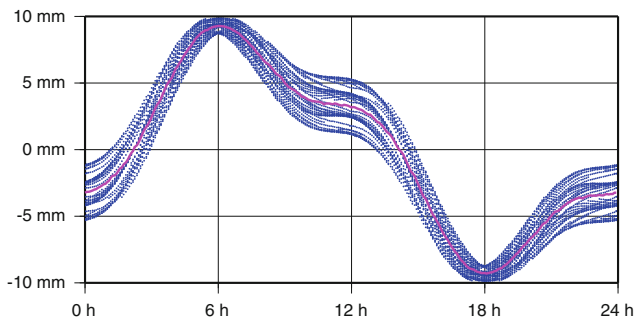
Fig. 6 Signature of a 1 cm X geocenter shift on simulated observations made on a GPS-like satellite. Each *blue dot* represents an element of S_y. The *magenta line* is an epoch mean
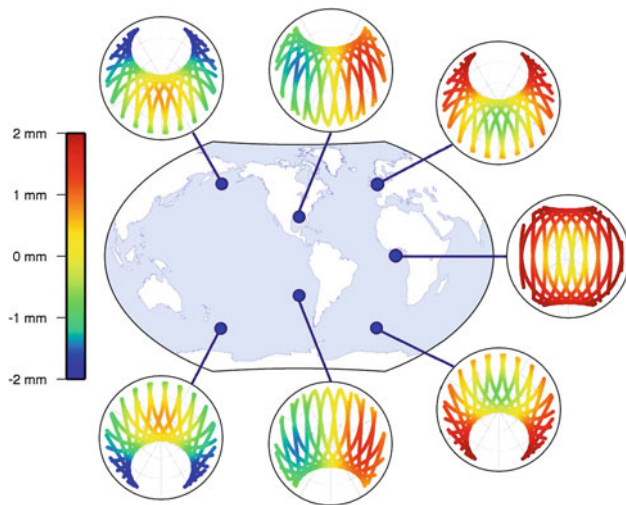

Fig. 7 Signature of a 1 cm X geocenter shift on simulated observations made by seven particular stations. An epoch mean signature was first removed for each satellite

around the magenta line in Fig. 4). This second-order signature is represented in Fig. 5 from the points of view of five particular stations.

5.2 Signatures of X and Y geocenter shifts

Similarly, the impact of a positive X geocenter shift is to shorten the observations made on satellites in the positive X hemisphere and to lengthen the observations made on satellites in the negative X hemisphere. At first order, the signature of a positive X geocenter shift on the observations of a particular satellite thus follows the opposite of the satellite X coordinate in the terrestrial frame. For a circular orbit, this results in the product of two sinusoids, one at the satellite revolution period and the other at the Earth rotation period. The signature of a 1 cm X geocenter shift on the set of observations described in Sect. 4.2 is represented in Fig. 6 from the point of view of a particular satellite.

As for the Z component, the epoch mean signature shown in magenta in Fig. 6 can be strictly compensated by variations

Table 4 List of simulated parameters

Type	Number
Station coordinates	3 per station
Satellite initial state vectors	6 per satellite
Satellite empirical accelerations	5 per satellite
EOPs	6

of the satellite clock offsets and is therefore unobservable in a standard GNSS analysis. The determination of the X component of the geocenter with GNSS can consequently only rely on the difference between its signature and this epoch mean signature (i.e. on the signal around the magenta line in Fig. 6). This second-order signature is represented in Fig. 7 from the points of view of seven particular stations.

The signature of a Y geocenter shift on station-satellite ranges is similar in all respects to the signature of an X geocenter shift.

6 SLR interlude

The collinearity diagnosis developed in Sect. 3 is applied in this section to the SLR geocenter determination problem. This interlude will help in understanding why the SLR technique is much more able to retrieve geocenter motions than GNSS.

6.1 Simulation

A series of station-satellite range observations was simulated with the options listed in Table 1, except that a constellation of two LAGEOS-like satellites ($a = 12,200$ km, $e = 0$, $i_1 = 110°$, $i_2 = 53°$) was used. A design matrix was set up, including the parameters listed in Table 4. The considered empirical accelerations were constant along-track accelerations and once-per-revolution periodic accelerations in the along-track and cross-track directions: S_0, S_c, S_s, W_c and W_s in the notations of Rodriguez-Solano et al. (2012). The main differences with the GNSS case is that neither clock offsets nor tropospheric parameters needed to be set up.

The choice of a perfectly distributed network of 100 stations providing observations at a 5 min rate is rather unrealistic for an SLR simulation. But like in the GNSS case, this choice avoids perturbing the obtained results by some network effect. This will also facilitate the comparison with the GNSS results obtained in Sect. 7.

The choice of a 24 h data span is also questionable, as 7 day data batches are usually processed in SLR. 24 h data batches were used for comparison with GNSS. But the results of additional simulations using 7 day data batches will also be presented in Sects. 6.2 and 6.3.
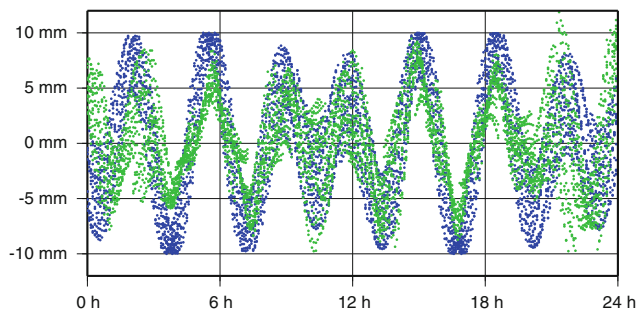
Fig. 8 *Blue* signature of a 1 cm *X* geocenter shift on simulated observations made on a LAGEOS-like satellite. Each *blue dot* represents an element of S_y. *Green* corresponding proper signature. Each *green dot* is an element of $S_{y,c}^p$

Fig. 9 *Blue* signature of a 1 cm *Z* geocenter shift on simulated observations made on a LAGEOS-like satellite. Each *blue dot* represents an element of S_y. *Green* corresponding proper signature. Each *green dot* is an element of $S_{y,c}^p$

6.2 Collinearity diagnosis of the *X* and *Y* geocenter coordinates

The implicit parameter corresponding to a 1 cm *X* geocenter shift was then considered, and Eq. (44) was solved. Concretely, a 1 cm *X* geocenter shift was imposed with respect to the a priori parameters. But the impact of this shift on the observations was compensated as much as possible through independent parameter variations. The VIF thus obtained for the *X* geocenter coordinate was 1.8 (67.068 %), which clearly indicates the absence of collinearity issues. This result is illustrated in Fig. 8, where the signature of the introduced *X* geocenter shift on the observations made on a particular satellite is compared to the corresponding proper signature. Both have similar magnitudes, meaning that the introduced *X* geocenter shift could hardly be compensated by independent parameter variations.

The same experience was repeated for the *Y* geocenter coordinate. An even lower VIF of 1.2 (42.698 %) was obtained. Additional simulations were carried out using a 7 day data batch. The obtained VIFs were respectively 1.04 (20.359 %) and 1.04 (19.078 %) for the *X* and *Y* geocenter coordinates. In conclusion, the determination of the *X* and *Y* geocenter coordinates with SLR does manifestly not suffer from collinearity issues.

6.3 Collinearity diagnosis of the *Z* geocenter coordinate

For the *Z* coordinate of the geocenter and a 24 h data batch, a larger VIF of 9.0 (94.285 %) was obtained. This result is illustrated in Fig. 9: the proper signature of the introduced *Z* geocenter shift is clearly smaller than its signature. The first-order sinusoidal signal could in particular be absorbed by independent parameter variations.

The examination of those independent parameter variations, i.e. $-\gamma_{y,c}$, revealed that the most affected parameters were the satellite initial state vectors. We therefore investi-
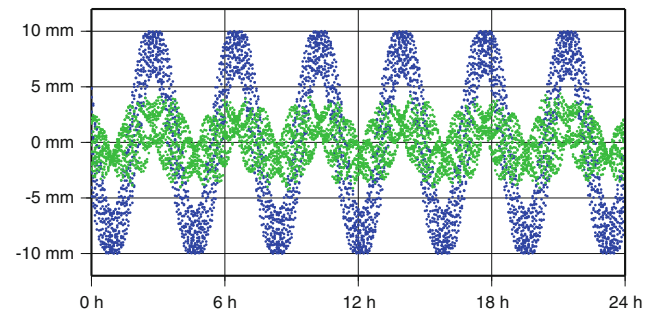
gated how variations of the satellite initial state vectors could have absorbed the first-order sinusoidal signature of the introduced *Z* geocenter shift. It is easily seen that this first-order signal can be compensated by a periodic variation of the orbit radius with:

– an amplitude of $\delta t \sin i$,
– its maximum when the satellite reaches the southernmost point of its orbit,
– its minimum when the satellite reaches the northernmost point of its orbit.

Starting from a circular orbit, such a periodic variation of the orbit radius can in fact simply be obtained through a slight "ellipticization". Let us arbitrarily place the perigee of the starting circular orbit at $\omega = \pi/2$ (i.e. at its northernmost point) and consider the perturbed orbit with an eccentricity $\delta e = \delta t \sin i / a$. The radial difference between both orbits is, at first order in δe:

$$\delta r = -a\delta e \cos \nu = -\delta t \sin i \cos \nu \tag{50}$$

It clearly meets the requirements listed above.

In summary, the first-order signature of a *Z* geocenter shift can be compensated, in case of circular orbits, by variations of the satellite osculating elements, or equivalently by variations of their initial state vectors. The parameter variation $-\gamma_{y,c}$ obtained from our simulation was indeed corresponding to such ellipticizations of both LAGEOS orbits. It is worth mentioning that this problem is not restricted to circular orbits. Appendix H (Online Resource) shows that the first-order signature of a *Z* geocenter shift can similarly be compensated by variations of the satellite osculating elements in case of elliptical orbits.

The same experience was repeated with a 7 day data batch. The VIF obtained for the *Z* geocenter coordinate was 8.6 (93.988 %), only slightly lower than for the 24 h case. The collinearity of the *Z* geocenter coordinate with the satellite osculating elements explained above holds in fact for any

data batch and orbital arc lengths. In addition to the uneven distribution of the SLR network, this slight collinearity issue may partly explain why the Z component of the SLR-derived geocenter motion is of lower quality than its X and Y components (see, e.g., Fig. 4 in Altamimi et al. 2011).

7 Collinearity diagnosis of the GNSS geocenter determination

The collinearity diagnosis developed in Sect. 3 is eventually applied in this section to the GNSS geocenter determination problem.

7.1 Collinearity diagnosis of the X and Y geocenter coordinates

A series of observations was simulated using the options listed in Table 1, and a design matrix including the parameters listed in Table 2 except satellite z-PCOs was set up. The implicit parameter corresponding to a 1 cm X geocenter shift was considered and Eq. (44) was solved. The obtained VIF was 2,367.5 (99.979 %). As illustrated from the point of view of a satellite in Fig. 10 and from the point of view of a station in Fig. 11, the proper signature of the X geocenter coordinate is indeed smaller than its signature by almost two orders of magnitude.

The independent parameter variations $-\boldsymbol{\gamma}_{y,c}$ by which the introduced X geocenter shift was almost completely absorbed was then examined. As anticipated in Sect. 5, the epoch mean signature of the introduced geocenter shift on the observations of each satellite (magenta line in Fig. 6) was absorbed by the respective satellite clock offsets. As one could have expected, the second-order signatures represented in Fig. 7 were absorbed to a great extent by the station-related parameters (positions, clock offsets, ZWDs and tropospheric gradients). On the other hand, neither the
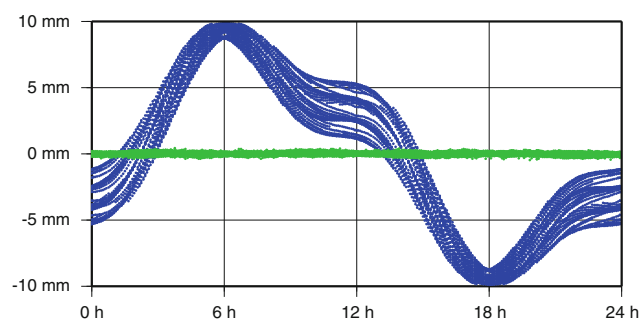
satellite initial state vectors nor the empirical accelerations were substantially affected.

Figure 12 illustrates the part of $-\boldsymbol{\gamma}_{y,c}$ corresponding to station coordinate variations, i.e. the distortion of the station network obtained in response to the introduction of the X geocenter shift. The distortion pattern visible in Fig. 12 resembles the deformation pattern associated with a degree 1, order 1 surface load (fitting a degree 1, order 1 load deformation pattern to the network distortion shown in Fig. 12 leads to a coefficient of determination of 94.5 %). This resemblance explains the significant correlation observed by Blewitt (personal communication, 2012) in the solutions of various IGS ACs between the X component of their origins and the deformation pattern associated with a degree 1, order 1 surface load.

The same experience was repeated for the Y coordinate of the geocenter. The obtained VIF was 2,359.8 (99.979 %). The independent parameter variations obtained in response to the introduction of the Y geocenter shift are similar to those obtained for the X coordinate of the geocenter. In particular,
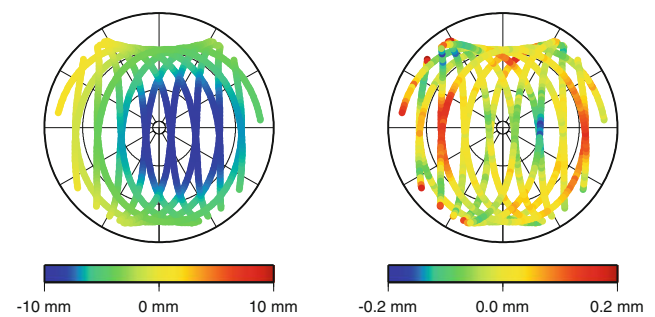

Fig. 11 *Left* signature of a 1 cm X geocenter shift on the observations made by a particular station, represented as a skyplot. Each *dot* represents an element of $\boldsymbol{S}_y$. *Right* corresponding proper signature. Each *dot* represents an element of $\boldsymbol{S}_{y,c}^p$. Note the different *color scales*

Fig. 10 *Blue* signature of a 1 cm X geocenter shift on simulated observations made on a GPS-like satellite. Each *blue dot* represents an element of $\boldsymbol{S}_y$. *Green* corresponding proper signature. Each *green dot* is an element of $\boldsymbol{S}_{y,c}^p$
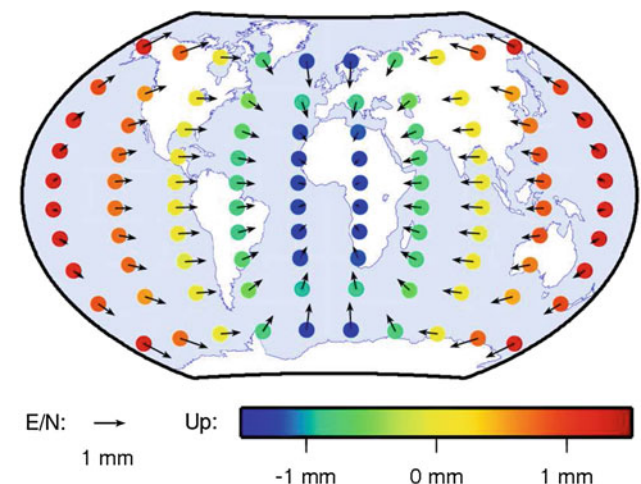

Fig. 12 Station coordinate variations obtained in response to the introduction of a 1 cm X geocenter shift. The horizontal variations are represented by the *black arrows*; the vertical variations by the *color dots*

the obtained network distortion pattern resembles the deformation pattern associated with a degree 1, order -1 surface load.

Two other simulations were run using a real network of 150 stations and a real constellation of 30 GPS satellites (both extracted from a solution provided by ESA for July 11, 2008). The obtained VIFs were, respectively, 2,016.4 (99.975 %) and 2,270.2 (99.978 %) for the X and Y coordinates of the geocenter. Although slightly lower, they are of the same order as the VIFs obtained with perfectly distributed network and constellation.

In conclusion, the X and Y coordinates of the geocenter are hardly observable in a standard GNSS analysis. Their epoch mean signatures are indeed indistinguishable from the satellite clock parameters, while their second-order signatures are highly collinear with all station-related parameters. The determination of the X and Y geocenter coordinates with GNSS can therefore only rely on tiny third-order signals (a few tenths of millimeters for 1 cm geocenter shifts). Note that the VIFs obtained for the X and Y geocenter coordinates are roughly of the same order as the VIF obtained in Sect. 4.3 for the terrestrial scale.

7.2 Collinearity diagnosis of the Z geocenter coordinate

Using a fictive network of 100 stations and a fictive constellation of 24 satellites, a VIF of 3,147.5 (99.984 %) was obtained for the Z coordinate of the geocenter. Using a real network of 150 stations and a real constellation of 30 GPS satellites, the obtained VIF was 3,538.4 (99.986 %). The examination of $-\boldsymbol{\gamma}_{y,c}$ revealed that both the clock offsets (as for the X and Y geocenter coordinates) and the initial state vector of each satellite (as in the SLR case) "combined their strengths" to absorb the main part of the signature of the introduced Z geocenter shift. As for the X and Y coordinates, the remaining second-order signature was largely absorbed by variations of the station-related parameters, leaving a proper signature of

only a few tenths of millimeters. The network distortion pattern obtained in response to the introduction of the Z geocenter shift resembles the deformation pattern associated with a degree 1, order 0 surface load.

As will be shown in Sect. 7.4, the larger VIFs of the Z geocenter coordinate compared to those of the X and Y geocenter coordinates stem from a particular role played by the ECOM parameters. The VIFs obtained for the Z geocenter coordinate are of the same order as those obtained in Sect. 4.3 for the terrestrial scale. This concretely means that current GNSS should be considered as unable to provide information about the Z component of geocenter motion as they are to provide terrestrial scale information apart from conventional satellite z-PCOs.

7.3 Influence of the cutoff angle and of the observation weighting

For completeness, the VIFs of the three geocenter coordinates have been computed for different cutoff angles and observation weighting functions. Results are summarized in Table 5. As for the terrestrial scale, using higher cutoff angles or downweighting low-elevation observations has the effect of increasing collinearity issues.

7.4 Role of the empirical accelerations

Meindl et al. (2013), on the basis of orbital perturbation considerations, concluded that the estimation of the ECOM D_0 parameters (constant accelerations in the Sun-satellite directions) was an important limiting factor in the determination of the Z geocenter coordinate with GNSS. To investigate the role effectively played by the ECOM parameters in the collinearity of the Z geocenter coordinate, a series of simulations was run in which different subsets of ECOM parameters were estimated. The results are summarized in Table 6.

Table 5 VIFs obtained for the three geocenter coordinates with different cutoff angles and observation weighting functions

Weighting function	Cutoff angle			
	0°	5°	10°	20°
1	X: 451.8 (99.889 %)	X: 1,070.1 (99.953 %)	X: 2,367.5 (99.979 %)	X: 12,475.9 (99.996 %)
	Y: 452.4 (99.889 %)	Y: 1,073.4 (99.953 %)	Y: 2,359.8 (99.979 %)	Y: 12,494.0 (99.996 %)
	Z: 929.8 (99.946 %)	Z: 1,661.7 (99.970 %)	Z: 3,147.5 (99.984 %)	Z: 13,799.2 (99.996 %)
$\sin e$	X: 656.5 (99.924 %)	X: 1,277.3 (99.961 %)	X: 2,658.6 (99.981 %)	X: 13,585.8 (99.996 %)
	Y: 655.3 (99.924 %)	Y: 1,283.1 (99.961 %)	Y: 2,653.4 (99.981 %)	Y: 13,599.3 (99.996 %)
	Z: 1,300.9 (99.962 %)	Z: 2,008.0 (99.975 %)	Z: 3,570.5 (99.986 %)	Z: 15,035.1 (99.997 %)
$\sin^2 e$	X: 1,128.7 (99.956 %)	X: 1,950.6 (99.974 %)	X: 3,604.9 (99.986 %)	X: 16,211.1 (99.997 %)
	Y: 1,126.2 (99.956 %)	Y: 1,959.1 (99.974 %)	Y: 3,598.4 (99.986 %)	Y: 16,219.0 (99.997 %)
	Z: 2,016.1 (99.975 %)	Z: 2,921.4 (99.983 %)	Z: 4,794.7 (99.990 %)	Z: 18,004.7 (99.997 %)

The other simulation options were as described in Sect. 4.2, except that satellite z-PCOs were not estimated

Table 6 VIFs obtained for the Z coordinate of the geocenter when estimating different subsets of ECOM parameters

ECOM parameters	VIF	$\sqrt{1-1/\text{VIF}}$ (%)
None	2,549.1	99.980
D_0	2,550.7	99.980
Y_0	2,549.3	99.980
B_0	2,553.2	99.980
B_c, B_s	2,603.0	99.981
D_0, B_c, B_s	3,137.9	99.984
D_0, Y_0, B_0, B_c, B_s	3,147.5	99.984

The other simulation options were as described in Sect. 4.2, except that satellite z-PCOs were not estimated

Table 7 VIFs obtained for the Z coordinate of the geocenter when estimating different subsets of ECOM parameters and using the GLONASS-like constellation described in the text

ECOM parameters	VIF	$\sqrt{1-1/\text{VIF}}$ (%)
None	2,568.5	99.981
D_0	2,799.4	99.982
Y_0	2,569.4	99.981
B_0	2,578.8	99.981
B_c, B_s	2,608.7	99.981
D_0, B_c, B_s	4,756.7	99.989
D_0, Y_0, B_0, B_c, B_s	4,782.5	99.990

The other simulation options were as described in Sect. 4.2, except that satellite z-PCOs were not estimated

The purpose here was to assess the individual and combined contributions of the five usually estimated ECOM parameters to the collinearity of the Z geocenter coordinate. It is clear that, when individually estimated, each of these five parameters, in particular D_0, has no significant impact. When the five parameters are simultaneously estimated, the VIF of the Z geocenter coordinate increases from about 2,550 (99.980 %) to 3,147.5 (99.984 %). This increase can in fact be quasi-fully explained by the simultaneous estimation of three of the five parameters: D_0, B_c and B_s. It is nevertheless relatively minor (remember that VIFs should be considered as varying on a logarithmic scale). That is why we assert that the ECOM parameters do not play a predominant role in the problem of determining the Z geocenter coordinate with GNSS.

The results in Table 6 were however obtained with a particular configuration of the orbital planes with respect to the Sun. The β_s angles (elevations of the Sun above the orbital planes) were in this case ranging from $-30°$ to $68°$. To confirm the above conclusion, we ran another series of simulations using a configuration considered by Meindl et al. (2013) as a worst case scenario. A constellation of 24 GLONASS-like satellites ($a = 25,520$ km, $e = 0$, $i = 65°$) on three orbital planes was used. The β_s angles were respectively 87°,

Table 8 VIFs obtained for the three geocenter coordinates when estimating different subsets of GNSS-specific parameters

GNSS parameters	Axis	VIF	$\sqrt{1-1/\text{VIF}}$ (%)
None	X	1.0	16.238
	Y	1.0	16.512
	Z	33.4	98.490
ECOM	X	4.0	86.522
	Y	4.0	86.497
	Z	44.5	98.870
Tropo	X	2.4	76.107
	Y	2.4	76.082
	Z	36.4	98.617
Clocks	X	677.8	99.926
	Y	681.3	99.927
	Z	768.4	99.935
ECOM, tropo	X	6.5	92.043
	Y	6.6	92.067
	Z	55.9	99.101
ECOM, clocks	X	719.7	99.931
	Y	720.7	99.931
	Z	1,301.6	99.962
Tropo, clocks	X	2,308.5	99.978
	Y	2,300.3	99.978
	Z	2,549.1	99.980
ECOM, tropo, clocks	X	2,367.5	99.979
	Y	2,359.8	99.979
	Z	3,147.5	99.984

The other simulation options were as described in Sect. 4.2, except that satellite z-PCOs were not estimated

$-15°$ and $-15°$ for the three orbital planes. Results are summarized in Table 7. The VIF of the Z geocenter coordinate is this time approximately doubled when estimating the five ECOM parameters. As previously, this collinearity increase can be explained by the simultaneous estimation of only three ECOM parameters: D_0, B_c and B_s. But this increase by a factor 2 in a worst case scenario remains a secondary issue. Also, note that estimating only the D_0 parameters causes a marginal increase of collinearity.

A last experiment was carried out to consolidate our view. The parameters estimated in GNSS analyses, but not in SLR analyses were grouped into three categories:

- the five usually estimated ECOM parameters ("ECOM" in Table 8),
- tropospheric parameters (ZWDs and tropospheric gradients; "tropo" in Table 8),
- station and satellite clock offsets ("clocks" in Table 8).

Different simulations were run to assess the individual and combined contributions of these parameter categories to the collinearity of the three geocenter coordinates. The obtained VIFs are summarized in Table 8.

The GNSS parameter category with the largest individual impact is the clock offset category: a hypothetical GNSS that could dispense with the estimation of clock offsets would most certainly allow an accurate determination of geocenter motion. The combination of clock offsets with tropospheric parameters has a devastating effect. It concretely makes the second-order signatures shown in Figs. 5 and 7 quasi-unobservable. In case of the Z geocenter coordinate, estimating the five ECOM parameters has an additional, but relatively small impact. That is why we consider that the inability of GNSS, as opposed to SLR, to properly sense the Z component of geocenter motion is mostly due to the simultaneous estimation of clock offsets and tropospheric parameters. For the X and Y components of geocenter motion, this inability is quasi-entirely due to the simultaneous estimation of clock offsets and tropospheric parameters. This conclusion contradicts the one drawn by Meindl et al. (2013) according to whom the inability of GNSS, as opposed to SLR, to properly sense the Z component of geocenter motion stems from the correlation between the Z geocenter coordinate and the ECOM D_0 parameters.

8 Discussion

This section discusses a number of questions related to the results obtained in Sect. 7:

– Why did Meindl et al. (2013) come to a different conclusion (Sect. 8.1)?
– Why are GLONASS-derived geocenter time series of much lower quality than GPS-derived geocenter time series (Sect. 8.2)?
– Which paths can be considered toward a reliable observation of geocenter motion with GNSS (Sect. 8.3)?

8.1 Comments to Meindl et al. (2013)

The main argument of Meindl et al. (2013) relies on experiments that are similar in essence to our simulations. They compared two series of GNSS solutions obtained with and without constraining the Z geocenter coordinate, i.e. with and without introducing artificial δz geocenter shifts. And they observed that the variations of the estimated D_0 parameters in response to the introduction of δz geocenter shifts were approximately obeying:

$$\delta z = -\frac{\sum_{k=1}^{P} \delta D_0^k \sin \beta_s^k}{n^2 \cos i} \tag{51}$$

where

– P denotes the number of orbital planes,
– δD_0^k is the mean variation of the D_0 parameters observed for the satellites of plane k,
– β_s^k is the elevation of the Sun above the orbital plane k,
– n denotes the mean motion of the satellites.

Meindl et al. (2013) justify Eq. (51) by the fact that a variation δD_0 has the effect, among others, of translating the orbit of a satellite by $\delta D_0 \sin \beta_s / (n^2 \cos i)$ along the Z axis. From Eq. (51), they conclude that the geocenter differences δz between their two solution series are "explained by the differences of the $[D_0]$ parameters in both solution series".

We were however unable to reproduce Meindl et al. (2013)'s result. We introduced for example 1 cm Z geocenter shifts into two simulated solutions that were only differing by the employed cutoff angles ($0°$ in the first, $10°$ in the second). The obtained right-hand sides of Eq. (51) were respectively 2.3 and 5.3 mm, both far from 1 cm, and also very different from each other. Repeating the same experiment with 1 year of real daily solutions provided by ESA led to right-hand sides that were rather constant (mean 4.6 mm, standard deviation 1.0 mm), but again far from 1 cm. We therefore think that Eq. (51) does probably only hold for the particular analysis settings used by Meindl et al. (2013).

In fact, the point where the reasoning of Meindl et al. (2013) fails is that their δz geocenter differences are not *explained* by the δD_0 variations. On the contrary, these δD_0 variations are only one particular consequence of the introduction of the δz geocenter shifts. Introducing an artificial Z geocenter shift into a solution admittedly induces variations of the D_0 parameters. But all other parameter categories are affected as well. With given analysis settings, formulas like Eq. (51) could in fact be derived for any parameter category like, e.g., tropospheric gradients. But each would only give a partial view of the problem.

8.2 Lower quality of GLONASS-derived geocenter time series

The Z component of the GLONASS-derived geocenter time series studied by Meindl et al. (2013) is clearly of much lower quality than the corresponding GPS-derived time series. It contains in particular a strong artificial periodic signal with an amplitude of about 20 cm and its extrema when the angle β_s reaches extremal values for one of the three GLONASS orbital planes. Meindl et al. (2013) attribute this lower quality to the facts that GLONASS satellites are spread over only three orbital planes (against 6 for GPS) and that the angle β_s can reach values up to almost $90°$ for GLONASS (against about $80°$ for GPS).

But the lower quality of GLONASS-derived geocenter time series might have a different explanation. According to Meindl (2011), less than 50 % of the phase cycle ambiguities could indeed be fixed to integer values in their GLONASS analysis (against 90 % for GPS). Unfixed ambiguities thus constitute a large set of additional parameters in the GLONASS case, which may have seriously increased the collinearity of the Z geocenter coordinate. No dedicated simulations were carried out in our study to assess the impact of estimating unfixed ambiguities on the VIF of the Z geocenter coordinate. But ambiguity parameters (i.e. constants per pass of each satellite over each station) would likely significantly help in masking the second-order geocenter signatures shown in Fig. 5.

Also, note that the impact of fixing ambiguities on the GPS geocenter determination had been studied by Springer (2000). His figure 5.7 (b) shows the impact of fixing ambiguities on the Z component of the geocenter motion derived from GPS solutions. In the early part of the graph, when GPS ambiguities were not fixed, a strong artificial periodic signal with an amplitude of about 20 cm is visible, like in Meindl et al. (2013)'s GLONASS series.

8.3 Perspectives

The collinearity diagnosis made in Sect. 7 explains *why* the time series of translations derived from the IGS AC weekly solutions are far from reflecting a realistic geocenter motion. To paraphrase Belsley et al. (1980), the extreme collinearity of the three geocenter coordinates indeed results in a situation in which the systematic influence of geocenter motion on GNSS observations is swamped by the observation and modeling errors.

A different problem is to know *what* the IGS AC translation time series do actually reflect, i.e. what are the modeling deficiencies which contaminate the GNSS geocenter motion estimates. From the fact that the IGS AC translation time series contain strong spurious signals at harmonics of the GPS draconitic year, and from various experiments showing that changes in orbit modeling have significant impacts on GPS-derived geocenter motion (Springer 2000; Hugentobler and Marel 2006; Rodriguez-Solano et al. 2011), it seems clear that orbit modeling deficiencies are a major source of geocenter contamination. But other modeling aspects of the GNSS observations are also known to have serious impacts on GPS-derived geocenter motion, like the modeling of higher-order ionospheric effects (Petrie et al. 2010; Garcia-Fernandez et al. 2012).

Two paths can consequently be considered in view of a reliable observation of geocenter motion with GNSS: the reduction of collinearity issues and the reduction of modeling deficiencies. With the current state of collinearity, the latter solution would probably require immense progress in the modeling of orbit dynamics as well as in other modeling aspects. Remembering that the determination of a 1 cm geocenter offset relies on a signal of a few tenths of millimetres, it seems unlikely that modeling progresses alone will allow a reliable observation of geocenter motion with GNSS in the near term.

The other alternative is the reduction of collinearity issues, i.e. a reduction of the number of parameters to estimate. Bearing in mind that the most problematic parameter categories are clock offsets and tropospheric parameters, two paths can again be considered. The first one would be an improvement of global meteorological models up to a point where GNSS analyses could dispense with the estimation of tropospheric parameters, which also seems unfeasible in the near term.

The last remaining prospect is the modeling of station and/or satellite clocks by other means than epoch-wise offsets. The modeling of satellite clocks is especially attractive. If the time evolution of satellite clock offsets could be tightly constrained, then the epoch mean signatures of geocenter shifts (magenta lines in Figs. 4 and 6) could indeed become observable. The whole question is then to know how many satellites should carry stable clocks and how stable these clocks should be. This question will be the topic of a future study.

9 Summary

A collinearity diagnosis was developed, based on a generalization of the notion of variance inflation factor. It allows to assess and explain the collinearity of any explicit or implicit parameter in the presence of singularities supplemented by minimal constraints. Such a diagnosis can be practically performed by solving the constrained least-squares system (44): a unit error in the considered parameter is artificially introduced, but the impact of this error on the observations is compensated as much as possible by independent parameter variations.

This collinearity diagnosis was applied in Sect. 6 to the SLR geocenter determination problem. It revealed that the determination of the X and Y geocenter coordinates with SLR does not suffer from any collinearity issue. On the other hand, the epoch mean signature of a Z geocenter shift was shown to be absorbable by variations of the satellite initial state vectors. The Z geocenter coordinate thus has a VIF of the order of 9 in our simulated SLR analyses. In addition to the uneven distribution of the SLR network, this slight collinearity issue may partly explain why the Z component of the SLR-derived geocenter motion is of lower quality than its X and Y components.

In Sect. 7, the developed collinearity diagnosis was applied to the GNSS geocenter determination problem. A minimalist set of GNSS parameters was considered. With

reasonable cutoff angles and observation weighting functions, the VIFs obtained for the Z geocenter coordinate are at the same level, or larger than those obtained for the terrestrial scale in Sect. 4. Current GNSS should therefore be considered as unable to provide information about the Z component of geocenter motion as they are to provide terrestrial scale information apart from conventional satellite z-PCOs. The VIFs of the X and Y geocenter coordinates are smaller, but of the same order. It can be concluded without much exaggerating that current GNSS are insensitive to any component of geocenter motion.

Among the parameters considered in this study, two specific categories quasi-fully explain the insensivity of GNSS to the X and Y geocenter coordinates: epoch-wise clock offsets and tropospheric parameters. These two parameter categories also explain most of the insensivity of GNSS to the Z geocenter coordinate, which is in addition slightly amplified by the simultaneous estimation of three ECOM parameters: D_0, B_c and B_s. We therefore assert that the inability of GNSS, as opposed to SLR, to properly sense geocenter motion, including its Z component, is due to the simultaneous estimation of clock offsets and tropospheric parameters.

The possible paths toward a reliable observation of geocenter motion with GNSS were considered in Sect. 8.3. As sufficient progress in any of these paths can hardly be expected soon, the ultimate conclusion of this article is that GNSS will likely not become able to complement SLR for geocenter determination with the network shift approach in a reasonably near future. The IGS might consequently consider abandoning the idea of providing GNSS geocenter estimates in favour of adopting a conventional a priori geocenter motion model.

References

Altamimi Z, Collilieux X, Métivier L (2011) ITRF2008: an improved solution of the international terrestrial reference frame. J Geodesy 85(8):457–473. doi:10.1007/s00190-011-0444-4

Argus DF (2012) Uncertainty in the velocity between the mass center and surface of Earth. J Geophys Res 117(B10405). doi:10.1029/2012JB009196

Beckley BD, Lemoine SG, Luthcke SB, Ray RD, Zelensky NP (2007) A reassessment of global and regional mean sea level trends from TOPEX and Jason-1 altimetry based on revised reference frame and orbits. Geophys Res Lett 34(14):L14608. doi:10.1029/2007GL030002

Belsley DA (1991) A guide to using the collinearity diagnostics. Comput Sci Econ Manage 4(1):33–50

Belsley DA, Kuh E, Welsch RE (1980) Regression diagnostics: identifying influential data and sources of collinearity. Wiley, New York

Beutler G, Brockmann E, Gurtner W, Hugentobler U, Mervart L, Rothacher M, Verdun A (1994) Extended orbit modeling techniques at the CODE processing center of the International GPS service for geodynamics (IGS): theory and initial results. Manuscr Geod 19(6):367–386

Blaha G (1971) Inner adjustment constraints with emphasis on range observations. Tech. Rep. 148, Department of Geodetic Science, The Ohio State University, Columbus

Blewitt G, Lavallée D, Clarke P, Nurutdinov K (2001) A new global mode of Earth deformation: seasonal cycle detected. Science 294(5550):2342–2345. doi:10.1126/science.1065328

Cardellach E, Elósegui P, Davis JL (2007) Global distortion of GPS networks associated with satellite antenna model errors. J Geophys Res 112(B07405). doi:10.1029/2006JB004675

Chen G, Herring TA (1997) Effects of atmospheric azimuthal asymmetry on the analysis of space geodetic data. J Geophys Res 102(B9):20489–20502. doi:10.1029/97JB01739

Collilieux X, Wöppelmann G (2011) Global sea-level rise and its relation to the terrestrial reference frame. J Geodesy 85(1):9–22. doi:10.1007/s00190-010-0412-4

Collilieux X, Altamimi Z, Ray J, van Dam T, Wu X (2009) Effect of the satellite laser ranging network distribution on geocenter motion estimation. J Geophys Res 114(B04402). doi:10.1029/2008JB005727

Collilieux X, Métivier L, Altamimi Z, van Dam T, Ray J (2011) Quality assessment of GPS reprocessed terrestrial reference frame. GPS Solut 15(3):219–231. doi:10.1007/s10291-010-0184-6

Collilieux X, Altamimi Z, Argus DF, Boucher C, Dermanis A, Haines BJ, Herring TA, Kreemer CW, Lemoine FG, Ma C, MacMillan DS, Mäkinen J, Métivier L, Ries J, Teferle FN, Wu X (2013) External evaluation of the Terrestrial Reference Frame: report of the task force of the IAG sub-commission 1.2. In: Rizos C, Willis P (eds) Proceedings of the XXV IUGG General Assembly. Springer, Berlin Heidelberg, International Association of Geodesy Symposia, vol 139 (in press)

Dong D, Yunck T, Heflin M (2003) Origin of the international terrestrial reference frame. J Geophysi Res 108(B4):2200. doi:10.1029/2002JB002035

Dow JM, Neilan RE, Rizos C (2009) The International GNSS Service in a changing landscape of Global Navigation Satellite Systems. J Geodesy 83(3–4):191–198. doi:10.1007/s00190-008-0300-3

Draper NR, Smith H (1998) Applied regression analysis, 3rd edn. Wiley, New York

Farrar DE, Glauber RR (1967) Multicollinearity in regression analysis: the problem revisited. Rev Econ Stat 49(1):92–107

Garcia-Fernandez M, Butala M, Komjathy A, Desai SD (2012) Intercomparison of approaches for modeling second order ionospheric corrections using GNSS measurements. Abstract G11B–0920 presented at 2012 Fall Meeting, AGU, San Francisco

Gobinddass ML, Willis P, de Viron O, Sibthorpe A, Zelensky NP, Ries JC, Ferland R, Bar-Sever Y, Diament M (2009a) Systematic biases in DORIS-derived geocenter time series related to solar radiation pressure mis-modeling. J Geodesy 83(9):849–858. doi:10.1007/s00190-009-0303-8

Gobinddass ML, Willis P, de Viron O, Sibthorpe A, Zelensky NP, Ries JC, Ferland R, Bar-Sever Y, Diament M, Lemoine FG (2009b) Improving DORIS geocenter time series using an empirical rescaling of solar radiation pressure models. Adv Space Res 44(11):1279–1287. doi:10.1016/j.asr.2009.08.00

Haitovsky Y (1969) Multicollinearity in regression analysis: comment. Rev Econ Stat 51(4):486–489

Hugentobler U, van der Marel H, Springer T (2006) Identification and mitigation of GNSS errors. In: Springer T, Gendt G, Dow JM (eds) Proceedings of IGS workshop

Marquardt DW (1970) Generalized inverses, ridge regression, biased linear estimation and nonlinear estimation. Technometrics 12(3):591–612

Meindl M (2011) Combined analysis of observations from different global navigation satellite systems. Geodätisch-geophysikalische Arbeiten in der Schweiz, Schweizerischen Geodätischen Kommission

Meindl M, Beutler G, Thaller D, Dach R, Jäggi A (2013) Geocenter coordinates estimated from GNSS data as viewed by perturbation theory. Adv Space Res 51(7):1047–1064. doi:10.1016/j.asr.2012.10.026

Montgomery DC, Peck EA, Vining GG (2012) Introduction to linear regression analysis, 5th edn. Wiley, New York

Morel L, Willis P (2005) Terrestrial reference frame effects on global sea level rise determination from TOPEX/Poseidon altimetric data. Adv Space Res 36(3):358–368. doi:10.1016/j.asr.2005.05.11

Petit G, Luzum B (2010) IERS Technical Note 36. Verlag des Bundesamts für Kartographie und Geodäsie, Frankfurt-am-Main

Petrie EJ, King MA, Moore P, Lavallée DA (2010) Higherorder ionospheric effects on the GPS reference frame and velocities. J Geophys Res 115(B03417). doi:10.1029/2009JB006677

Ray J, Altamimi Z, Collilieux X, van Dam T (2008) Anomalous harmonics in the spectra of GPS position estimates. GPS Solut 12(1):55–64. doi:10.1007/s10291-007-0067-7

Ray JR, Rebischung P, Schmid R (2013) Dependence of IGS products on the ITRF datum. In: Altamimi Z, Collilieux X (eds) Reference frames for applications in geosciences. Springer, Berlin Heidelberg, International Association of Geodesy Symposia, vol 138, pp 63–67. doi:10.1007/978-3-642-32998-2_11

Rebischung P, Griffiths J, Ray J, Schmid R, Collilieux X, Garayt B (2012) IGS08: the IGS realization of ITRF2008. GPS Solut 16(4):483–494. doi:10.1007/s10291-011-0248-2

Rodriguez-Solano CJ, Hugentobler U, Steigenberger P, Lutz S (2011) Impact of Earth radiation pressure on GPS position estimates. J Geodesy 86(5):309–317. doi:10.1007/s00190-011-0517-4

Rodriguez-Solano CJ, Hugentobler U, Steigenberger P (2012) Adjustable box-wing model for solar radiation pressure impacting GPS satellites. Adv Space Res 49(7):1113–1128. doi:10.1016/j.asr.2012.01.016

van der Sluis A (1969) Condition numbers and equilibration of matrices. Numer Math 14(1):14–23

Springer TA (2000) Modeling and validating orbits and clocks using the Global Positioning System. Geodätisch-geophysikalische Arbeiten in der Schweiz, Schweizerischen Geodätischen Kommission

Springer TA, Beutler G, Rothacher M (1999) A new solar radiation pressure model for the GPS satellites. GPS Solut 2(3):50–62. doi:10.1007/PL00012757

Wu X, Collilieux X, Altamimi Z, Vermeersen BLA, Gross RS, Fukumori I (2011) Accuracy of the International Terrestrial Reference Frame origin and Earth expansion. Geophys Res Lett 38(13):L13304. doi:10.1029/2011GL047450

Wu X, Ray J, van Dam T (2012) Geocenter motion and its geodetic and geophysical implications. J Geodyn 58:44–61. doi:10.1016/j.jog.2012.01.00

Zhu SY, Massmann FH, Yu Y, Reigber C (2003) Satellite antenna phase center offsets and scale errors in GPS solutions. J Geodesy 76(11–12):668–672. doi:10.1007/s00190-002-0294-1